Thesis for the degree of Licentiate of Engineering

On the Design Considerations for Thermal Energy Storage with Phase Change Materials:

Material characterization and Modelling

Pepe Tan

Department of Architecture and Civil Engineering
Division of Building Technology
CHALMERS UNIVERSITY OF TECHNOLOGY
Göteborg, Sweden 2018

On the Design Considerations for Thermal Energy Storage with Phase Change Materials:
Material characterization and Modelling
Pepe Tan

Licentiatavhandlingar vid Chalmers tekniska högskola

Department of Architecture and Civil Engineering
Division of Building Technology
Chalmers University of Technology
SE–412 96 Göteborg, Sweden
Telephone + 46 (0) 31 – 772 1000

Typeset by the author using LaTeX.

Printed by Chalmers Reproservice
Göteborg, Sweden 2018

Abstract

Integrating thermal energy storage (TES) technologies to a process enables storing and releasing thermal energy on demand. Depending on the implementation, this may lead to economic and ecological improvements, e.g. by shifting the peak demand to off-peak hours or by increasing the share of utilized renewable energy. Additionally, the utilization of the latent heat of melting and solidification of so called phase change materials (PCMs) as storage materials offers the potential for considerably increased energy storage densities compared to materials storing only sensible heat.

This thesis summarizes current progress for developing a design framework, which covers the selection, utilization and process integration of a PCM TES. For selecting the material based on its phase change temperature and latent heat content, the T-History method has been developed further by studying the method numerically and experimentally. It is shown that adjustments in the data evaluation method have to be made in order to obtain repeatable measurement results. The results are then still subject to systematic errors, which limit the accuracy of the method.

In the next part, the material level results serve as model input to simulate charging or discharging cases of a PCM TES by modeling the heat transfer between the PCM and a heat transfer fluid (HTF). The developed model performs comparable to existing literature models but has to be verified experimentally in future work.

Based on the preliminary model, a process integration case is studied in terms of variations of geometrical and operational parameters relevant for the heat transfer within the PCM TES during (dis)charging. It is shown that restrictions given by the process may limit the effectiveness of a PCM TES considerably, if the PCM TES is operated at too high mass flow rates. It is concluded that the current results have to be placed at least within an economical context given by the process conditions in order to decide which PCM TES design is optimal.

Keywords: Phase Change Materials, Thermal Energy Storage, T-History, Simulation

Acknowledgments

This Licentiate thesis is the outcome of an ongoing PhD project that started out in June of 2015. The project was created based on funding by the Swedish Energy Agency (Energimyndigheten) and the Swedish Centre for Innovation and Quality in the Built Environment (IQ Samhällsbyggnad) together with Vesam AB within the E2B2 program (Forskning och innovation för energieffektivt byggande och boende).

It received further funding from the Chalmers Energy Area of Advance and the Swedish Environmental Protection Agency (Naturvårdsverket).

Foremost, I would like to thank my supervisors Angela Sasic Kalagasidis and Pär Johansson for their guidance over these years. The project wouldn't be where it is now without their continuous support, patience and many helpful suggestions. I am grateful for their advance in trust by choosing me as their PhD student.

Thanks also go to colleagues of the Division of Building Technology for their help during daily work. In particular to Marek Machowski, for his assistance when preparing experiments and to Kaj Pettersson, for his help regarding questions on numerical parts of the work.

I thank Per Löveryd of Akademiska Hus and the project members from ÅF for the helpful discussions during many project meetings and for providing the project with an interesting case to study. Participation within the IEA ECES Annex 30 (Energy Conversation through Energy Storage: Thermal Energy Storage for Cost-Effective Energy Management and CO_2 Mitigation) also contributed to the structure of the framework. Climator AB and Rubitherm GmbH have my thanks for providing PCM samples.

Stephan Vidi and Michael Brütting from the thermal analysis group of the Bavarian Center for Applied Energy Research (ZAE Bayern) have my special thanks for their hospitality during a study visit and for their insight on PCM characterization.

At last, thank you to my family, for being the best pillar of support I could have wished for.

Pepe Tan
Göteborg, January 2018

List of Publications

Appended to this thesis are the following papers:

Paper 1. Pepe Tan, Michael Brütting, Stephan Vidi, Hans-Peter Ebert, Pär Johansson, Helén Jansson, Angela Sasic Kalagasidis. *Correction of the enthalpy–temperature curve of phase change materials obtained from the T-History method based on a transient heat conduction model.* International Journal of Heat and Mass Transfer, Vol. 105, p. 573-588, 2017.

Paper 2. Pepe Tan, Michael Brütting, Stephan Vidi, Hans-Peter Ebert, Pär Johansson, Angela Sasic Kalagasidis. *On the factors influencing the accuracy and precision of the enthalpy-temperature curve obtained from the T-History method based on different experimental setups.* submitted to Thermochimica Acta, Nov. 2017. (Under Review)

Paper 1 investigates the T-History method for measuring the latent heat of solidification and melting of PCMs as well as the phase change temperature. Based on a numerical study it is shown that the current mathematical model causes a systematic overestimation of the sensible specific heat capacities and an underestimation of the latent heat, if the insulation thermal mass is neglected.
Contribution: The first author developed the methodology and wrote the paper. The modeled experiment was based on the experimental setup used at ZAE Bayern. The remaining authors contributed with interpretation of the results, editing and revising the manuscript.

Paper 2 contains a study of different experimental setups for the T-History method. Relevant factors influencing the measurement accuracy and precision are discussed. It is shown that the time derivative of the temperature over time data should be cleared from noise carefully in order not to over- or underestimate the latent heat. Moreover, a smaller sample mass compared to the sample holder and insulation leads to a systematic underestimation of the latent heat. This result supports the conclusion made in Paper 1.
Contribution: The first author developed the methodology, carried out the experiment and wrote the paper. The same experimental setup is used as at ZAE Bayern. The remaining authors contributed with editing and revising the manuscript.

List of Symbols

List of Abbreviations

amb	Ambient
FVM	Finite volume method
HTF	Heat transfer fluid
L	Liquid phase
PCM	Phase change material
ref	Reference material
S	Solid phase
t	Sample holder tube
TES	Thermal Energy Storage
WALL	Wall between phase change material and heat transfer fluid

List of Greek Symbols

α	Under-relaxation factor (-)
δ	Storage density ($\mathrm{J\,m^{-3}}$)
ϵ	Void factor (-)
η	Efficiency (-)
λ	Thermal conductivity ($\mathrm{W\,m^{-1}\,K^{-1}}$)
ρ	Density ($\mathrm{kg\,m^{-3}}$)
σ	Standard deviation
ω	Power to capacity ratio ($\mathrm{s^{-1}}$)

List of Roman Symbols

A	Area ($\mathrm{m^2}$)

c_p	Specific heat capacity ($\mathrm{J\,kg^{-1}\,K^{-1}}$)
e	T-History correction factor for heat flux (-)
H	Enthalpy (J)
h	Specific (mass or volume) enthalpy ($\mathrm{J\,kg^{-1}}$ or $\mathrm{J\,m^{-3}}$)
h_{WALL}	Forced convection heat transfer coefficient at the HTF and WALL boundary ($\mathrm{W\,m^{-2}\,K^{-1}}$)
L	Latent heat of melting and solidification ($\mathrm{J\,kg^{-1}}$)
L_{ch}	Characteristic length (m)
m	Mass (kg)
$\dot{m}$	Mass flow rate ($\mathrm{kg\,s^{-1}}$)
P	Power (W)
p	Pressure (Pa)
Q	Storage capacity (J)
$\dot{Q}$	Heat flux (W)
$\dot{q}$	Heat flux density ($\mathrm{W\,m^{-2}}$)
r	Radial coordinate (cylindrical geometry) (m)
R_{th}	Thermal resistance ($\mathrm{K\,W^{-1}}$)
T	Temperature (°C)
t	Time (s)
U	Internal Energy (J)
u	Velocity ($\mathrm{m\,s^{-1}}$)
V	Volume ($\mathrm{m^3}$)
x	Axial coordinate (m)
y	Vertical coordinate (rectangular geometry) (m)
z	Orthogonal coordinate depending on geometry (cylindrical: r, rectangular: y) (m)

List of Figures

List of Tables

Contents

Part I

Summary

Chapter 1

Introduction

1.1 Background and Challenges

Increasing the use of thermal energy storage (TES) is seen as an important measure to reach current sustainability targets in the world [1, 2]. This is because of their potential benefits such as increasing the share of renewable energies in a process or enabling possibilities for demand side management [3–5]. A process may especially benefit from a TES, if the availability of its energy sources is not aligned with its energy demand. Even more so if the energy prices differ considerably between low and high energy demand periods.

Tab. 1.1 lists commonly discussed concepts of storing thermal energy. Among them, the utilization of the latent heat of solidification and melting of so called phase change materials (PCMs) has been discussed for TES applications [6–9].

Table 1.1: Overview of different TES concepts given by [3].

Concept	Storage parameter	Technology level	Example
Sensible heat	$c_p \cdot \Delta T$ in $\mathrm{J\,kg^{-1}}$	Commercially available	Hot/cold water tank, Rock bed storage
Latent heat	L, $c_p \cdot \Delta T$ in $\mathrm{J\,kg^{-1}}$	Demonstration projects to commercially available (mostly ice storage)	Solid to liquid transition of PCMs (see Tab. 1.2)
Thermochemical	Heat of reaction/sorption	R&D stage	Metal sulphate reaction systems, Silica gel/water & Zeolite/water sorption systems

Tab. 1.2 lists material properties of common commercially available materials, which melt in a temperature range of building applications. They are jointly referred to as PCM, but can be classified further as organic (paraffins) or inorganic (salt hydrates).

When the PCM changes its state from solid to liquid (see Fig. 1.1) a significant amount of heat is stored by the material in form of its latent heat of melting and solidification: L ($\mathrm{kJ\,kg^{-1}}$) (see Tab. 1.2). When evaluated over the same temperature difference, the storage capacity increases significantly compared to a material storing only sensible heat (see Fig. 1.2).

Theoretically, this allows higher achievable storage densities, which becomes relevant if space is a limiting factor in building applications. The temperature difference in turn is given by the available heat sources and sinks of the process, through which the TES can be charged or discharged.

Table 1.2: Typical properties of (commercially available) PCMs for building applications (Temperature range: −10..100 °C). More material classes and detailed classifications can be found in [6–8, 10, 11].

	ρ in $\mathrm{kg\,m^{-3}}$	c_p in $\mathrm{J\,kg^{-1}\,K^{-1}}$	L in $\mathrm{kJ\,kg^{-1}}$	λ in $\mathrm{W\,m^{-1}\,K^{-1}}$
Water	1000	4180	330	0.6
Paraffins	ca. 700-900	ca. 2000	ca. 150-250	ca. 0.2
Salt Hydrates	ca. 1300-1500	ca. 2000	ca. 150-250	ca. 0.4-0.6

(a) Liquid state (b) Solid state

Figure 1.1: Phase change of two commercial PCMs (left sample holder: salt hydrate, right sample holder: paraffin)

In this work, only so called active TES are considered, which allow a process operator to control the state of charge by transferring heat between the storage material and the process applications via a heat transfer fluid (HTF) (typically water or air for building applications) [6, 12, 13]. This is opposed to passive applications, where the PCM is simply incorporated to building components (such as walls) in order to effectively increase its heat storage capacity [12].

The TES can then be essentially seen as a heat exchanger between the available heat sources and sinks of the process. The transfer of thermal energy then occurs on demand and is independent of the simultaneous availability of the latter (see Fig. 1.3).

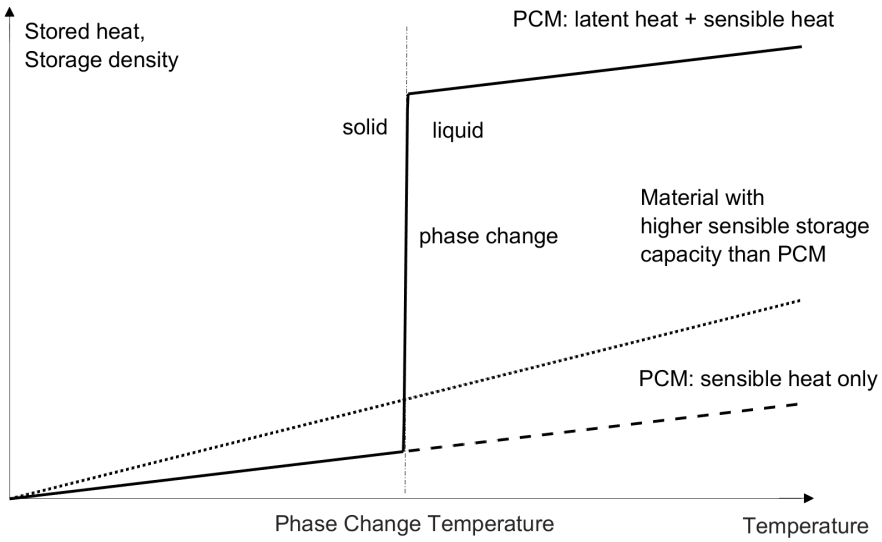

Figure 1.2: Illustration of the storage potential of a (solid-liquid) phase change.

The rate of heat transferred to or from the TES to the process sources and sinks then depends on the HTF mass flow rate and temperature difference at the TES in- and outlet. The maximum temperature difference between the charged and discharged state of the TES is given by the difference of charging and discharging temperatures at the TES inlet, respectively.

$$P^{TES} = \dot{m}_{HTF}\, c_p^{HTF} \Delta T \tag{1.1}$$

The amount of heat transferred for a given time is given by:

$$Q^{TES} = \int_0^t P^{TES} \mathrm{d}t \tag{1.2}$$

In order to fully utilize the latent heat storage potential, the TES then has to be carefully designed with respect to the given process conditions and requirements. This is because common PCMs in the temperature range of building applications have a lower sensible specific heat capacity compared to water as sensible heat storage material (e.g. $c_p^{paraffins} \approx 2000\ \mathrm{J\,kg^{-1}\,K^{-1}} < c_p^{water} \approx 4180\ \mathrm{J\,kg^{-1}\,K^{-1}}$, see Tab. 1.2).

The benefit of high storage densities using PCMs is therefore only given, if the latent heat can act on its own as a suitable heat source or sink with respect to the temperature levels of the process as shown in Fig. 1.4.

Considering that the costs for PCMs are considerably higher compared to other storage materials [14, 15], this makes it also a necessity for a PCM storage to be economically viable.

An additional challenge for designing the TES is given by the generally low thermal conductivity of PCMs (0.2-0.6 $\mathrm{W\,m^{-1}\,K^{-1}}$, see Tab. 1.2). This limits the

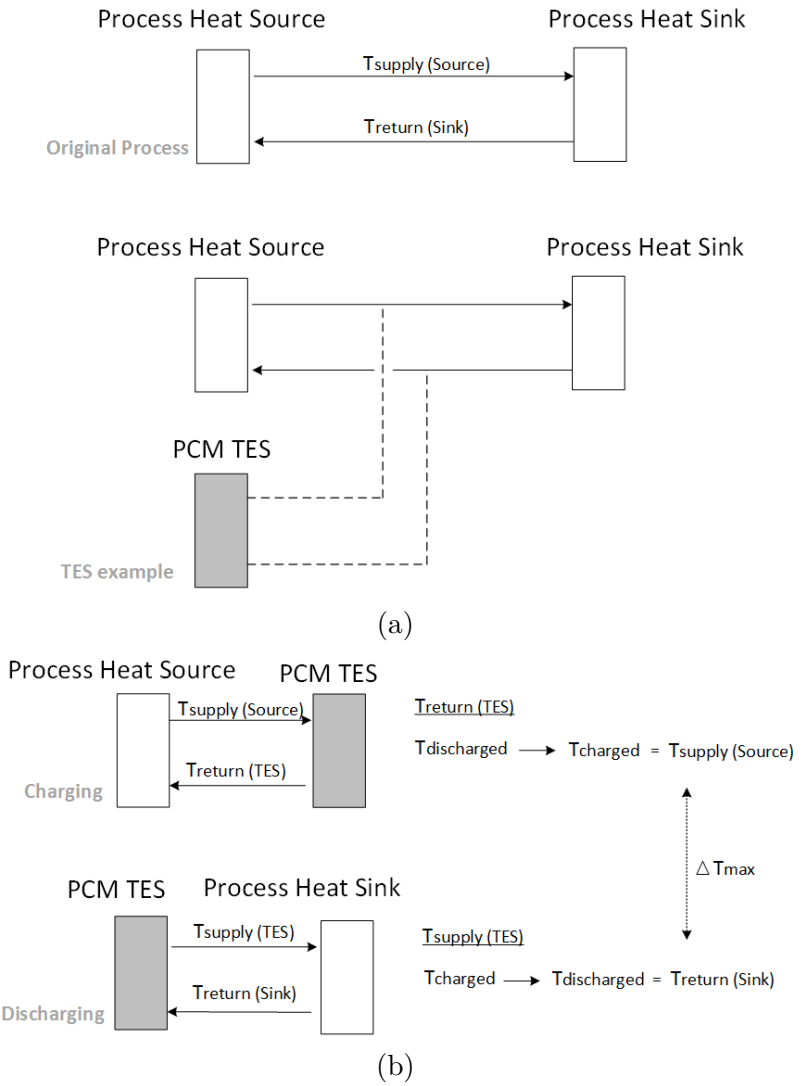

Figure 1.3: (a): Illustration of a TES integration: Heat is transferred first from the process heat source to the TES via a HTF during charging. For discharging, the heat is then supplied from the TES to the process heat sink. (b): Illustration of (dis)charging cases. When the TES is completely (dis)charged, the temperature inside the TES and of the HTF at the TES outlet will be equal to the provided process temperatures of the source/sink at the inlet of the TES. The difference between these two states is given as $\Delta T_{max} = \left| T_{supply}^{Source} - T_{return}^{Sink} \right|$.

achievable heat transfer rates between the PCM and the HTF and consequently the (dis)charge power, which the TES can provide to the process.

Each of the above challenges are still an active field of research. This ranges from material development and characterization [16, 17] to enhancing the heat transfer between the PCM and HTF [18] (e.g. via inclusion of fins). Literature for designing a PCM TES therefore are scattered and mostly focused on these single aspects. Moreover, it has to be checked whether they are applicable outside of the considered set of boundary conditions [19, 20].

It was also found that design guidelines listed in [19] are not evaluated with

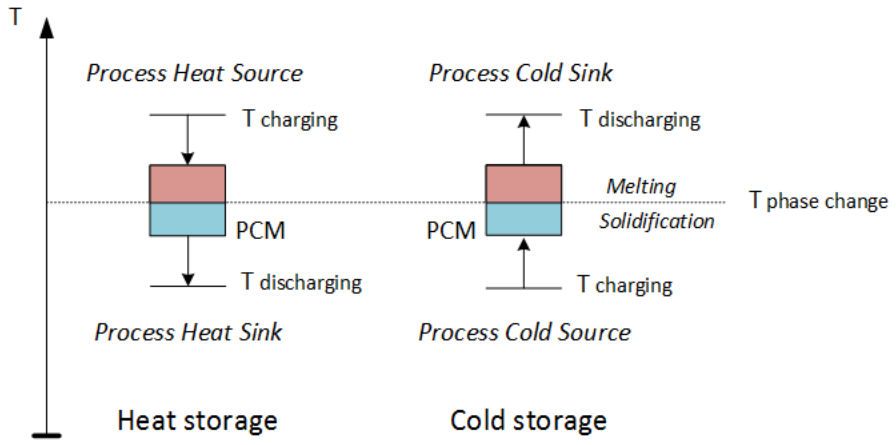

Figure 1.4: Illustration of the process temperature levels for (dis)charging a PCM as TES depending on a heat or cold storage application. Due to irreversibility of the (dis)charging processes, any heat and cold storage will supply the process heat/cold sink at a lower (heat storage) or higher (cold storage) temperature respectively, compared to the original process heat/cold source.

regards to process specific requirements. Since (dis)charging the TES is irreversible from a thermodynamic perspective [2, 21], the heat provided by the TES to the process heat/cold sinks are at inferior temperature levels compared to the process heat/cold sources (see Fig. 1.4). An important example would then be that the HTF at the outlet of the TES is able to meet a maximum or minimum temperature requirement in order to be usable by the process cold/heat sink.

Moreover, integrating any type of TES in a process is not a trivial task as it essentially involves defining a new process control strategy around the TES [22–25].

It is therefore clear that implementing any TES into a process requires a systematic definition and quantification of the benefits versus the costs of the TES, which stem from the design choices made. The development of a design framework can therefore be seen as equivalent to developing tools and criteria that enable this decision making process.

Since the lack of these tools pose a practical challenge for integrating any TES in real scale processes, developing these is currently an active field of research [26–28].

The need for these tools was moreover confirmed following discussions with industry partners for integrating a PCM cold storage for the JSP2 office building and with other researchers within the IEA ECES Annex 30 group [28]. The latter aims to develop performance criteria, which allows different TES technologies (such as listed in Tab. 1.1) to be comparable. Ideally, these could then be applied for designing and characterizing a PCM cold storage in the JSP2 project. The suggested approach in this thesis is the response of the author, who participated in these two projects.

The aim of the project is multifold. The overall desired outcome is a design framework that guides through the decision making steps when integrating a PCM

TES for a specific process.

First, these decision making steps leading to a PCM TES integration are identified and structured into separate design levels. For each level, an individual contribution to currently used research methodologies is (to be) done in order to improve its suitability for the overall framework.

The framework is described in more detail in the next sections followed by a summary of the actual contributions and a discussion of the limitations of the framework.

1.2 Design Framework

The framework has been structured into three different levels, which are seen as relevant for the design process. This ranges from choosing the storage material, evaluating the heat exchanger design to the system integration of the PCM TES.

The different levels are interconnected as they provide necessary input data for the other levels. This is explained in the following:

1. ***Material Level***: Characterization and selection of a suitable PCM based on process requirements.

   A PCM will be primarily chosen based on its phase change temperature and latent heat content. The former will determine the available temperature differences from the process for the heat transfer between the HTF and PCM in the actual storage device for (dis)charging according to Fig. 1.4. The latent heat on the other hand will allow an evaluation of the achievable storage capacity and density as well as the specific storage costs.

   In order to obtain accurate values for these material properties, current measurement techniques have to be improved further.

2. ***Device Level***: Design of the TES and evaluation of heat transfer between HTF and PCM based on process requirements.

   Based on given temperature differences from the process and the selected PCM, the TES should utilize as much of its latent heat as possible to supply the process at a specified power and duration, while fulfilling process temperature requirements on the HTF.

   Focus on the device scale is therefore to estimate the heat transfer between PCM and HTF for at least rectangular or cylindrical geometries (see Fig. 1.5). These basic geometries have been selected as they represent the most commonly considered heat exchanger geometries in literature [20]. A methodology is then to be developed in order to determine the necessary dimensions of HTF and PCM sections for these basic geometries, which fulfill any given design targets in terms of power and storage capacity. The result of this stage allows a prediction of the operation characteristics of the PCM TES within the process

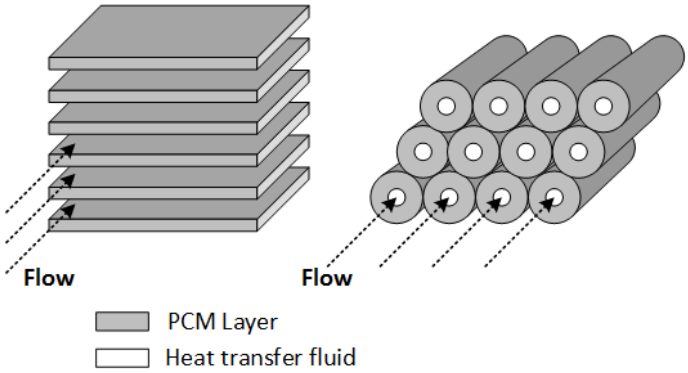

Figure 1.5: Illustration of two simplified TES geometries. Left: Flow of HTF over rectangular PCM plates; Right: Flow of HTF within tubes with surrounding PCM layer.

boundaries. These may additionally vary with different mass flow rates of the HTF for (dis)charging the PCM TES for the same geometry.

3. ***System Level***: Determination of the cost-optimum PCM TES size and control strategy for the given process.

   Since the PCM TES will be actively controllable, finding the optimum size and control strategy of the TES with respect to the given process will need an additional design methodology from a system level perspective. The control strategy essentially involves scheduling the (dis)charging occasions of the TES based on the availability of the process sources and sinks in order to maximize the economic and ecological net benefits of the process.

   This system level optimization places the material choice and TES device level design in context with its process integration. From the point of view of the author this is a crucial task for integrating any type of TES into a process.

   The outcome of this stage then provides the values of power and capacity of the storage that are to be used as design targets on the device level.

The outcome of the complete design framework should allow the user to evaluate and develop a PCM TES for their specific process from a technical and economic perspective. A flowchart summary is shown in Fig. 1.6.

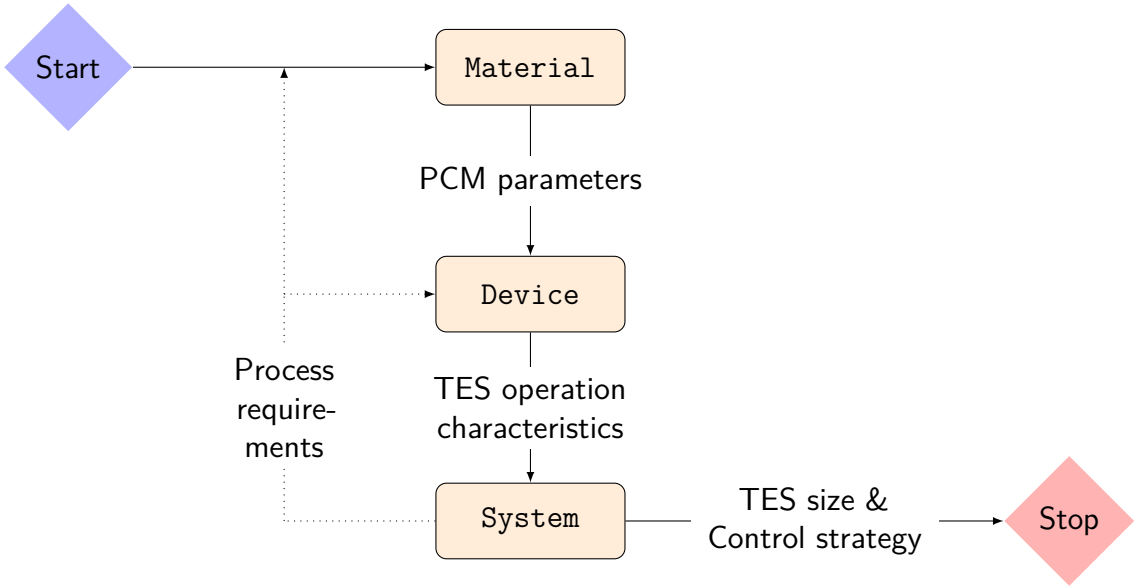

Figure 1.6: Illustrative flowchart of the design framework for a PCM TES

1.3 Thesis Outline

The next chapters of the thesis consist of a summary of the work done so far regarding the above framework. Preliminary results on material and device levels are presented in two separate parts of the thesis, while the methodology on system level is still subject to future work.

Measuring the latent heat and phase change temperature is still an active field of research because measurement standards are still in development. Among the established methods, the so called T-History method in particular has been based on a large variety of setups and data evaluation methods. The method is studied both numerically and experimentally in **Paper 1** and **Paper 2**, respectively. The overall aim of the work is to systematically improve the method by studying different experimental setups and proposing a suitable data evaluation algorithm. These findings are summarized in Chapter 2 and first measurements using PCMs are presented.

The measurement results of the latent heat and the phase change temperature can then be utilized on device level. In Chapter 3, a simplified simulation model of a PCM TES is presented based on the two geometries shown in Fig. 1.5. The model is compared against an existing literature model but has to be verified using own experimental results in the future. Based on how well the model agrees with future experimental data, it may then be necessary to extend the model further.

In Chapter 4, the model is applied on a cold storage integration example and its operation characteristics are studied using a set of proposed parameters based on the given process. Conclusions are then drawn in Chapter 5 on the future work necessary on system level.

1.4 Limitations

It is obvious that the reliability of the framework is subject to the individual limitations present in each of the mentioned levels. Fig. 1.7 shows this exemplary.

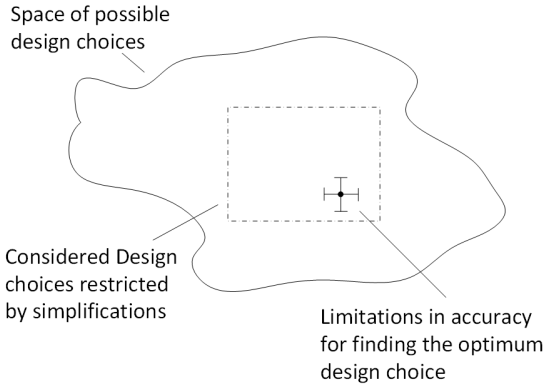

Figure 1.7: Illustration of the limitations

On material scale for example the reliability of choosing a PCM based on its material properties is limited by the accuracy of the measurement method itself. In this work, only the latent heat and phase change temperature was characterized. Other relevant material properties such as density and thermal conductivity are based on available literature values and have not been measured rigorously. It was moreover shown in **Paper 1** and **Paper 2** that the T-History method is still subject to systematic measurement errors, which have to be corrected in future work.

On device level, only two geometries for heat transfer between HTF and PCM are currently considered. The operation characteristics of the PCM TES should then be evaluated based on criteria, which may be applied in general terms. Ideally, this would make different heat transfer concepts using PCMs (e.g. a packed bed heat exchanger with PCM encapsulated in spheres [20]) and even other TES technologies comparable. This opens up more design choices and the designer may then find a more suitable TES for its process among the increased number of options. This is important in order not to exclude any suitable options in the first place.

However, any characteristics determined based on simulations or experimental results from smaller prototypes, can only be seen as approximations of its full scale performance. One difficulty is to attribute the origin of any model disagreements clearly to the uncertainties originating from material properties or to the simplifications in the model itself.

The outcome on system level is likely to be process specific and may then not be generally applicable to other TES integration cases. This is because the additional complexity of possible control choices depends on the process itself. And the main motivation of integrating a TES in the first place may differ depending on the initial process conditions. Since design guidelines are essentially tools for decision making, the complexity for developing these guidelines increases with the amount of possible decisions. Analyzing a PCM TES integration for an existing process offers for example less complexity compared to designing a complete new process including a TES. Then the sizing of the process sources and sinks may be additional variables.

Chapter 2

PCM Characterization using the T-History Method

2.1 Enthalpy measurements of PCMs

The state quantity enthalpy is commonly used for PCMs to quantify the energy stored in a material for a given temperature difference. From its definition and under the assumption that the system is at constant pressure, the enthalpy change of a material directly corresponds to the heat stored or released given by the 1st law of thermodynamics [6]:

$$\mathrm{d}U = \mathrm{d}Q - p\mathrm{d}V \tag{2.1a}$$

$$\mathrm{d}H = \mathrm{d}U + p\mathrm{d}V + V\mathrm{d}p \tag{2.1b}$$

$$\mathrm{d}H = \mathrm{d}Q \quad \text{for} \quad \mathrm{d}p = 0 \tag{2.1c}$$

It is therefore useful to plot the enthalpy change over the temperature range of a process in order to evaluate the storage potential of any material to be used for a TES. The mass specific enthalpy can be expressed via the mass specific (isobaric) heat capacity and the temperature change of the material:

$$\frac{\mathrm{d}h}{\mathrm{d}T} = c_p(T) \tag{2.2}$$

$$\Delta h_{1-2} = \int_{T_1}^{T_2} c_p(T)\mathrm{d}T \tag{2.3}$$

Available methods to derive the temperature dependent enthalpy curve, such as differential scanning calorimeters (DSC), are typically designed to measure the specific heat capacity in only solid or liquid phase of a material and not explicitly for phase change. Moreover, they are usually designed for pure materials [16]. Therefore typical simplifications are made when measuring PCMs:

- The latent heat is lumped together using an effective (or apparent) heat capacity c_p^{eff}. When the sample undergoes melting or solidification, the instrument sees an apparent peak of the specific heat capacity at the phase change temperature due to the additional storage or release of latent heat, respectively.

  Moreover, the mathematical models assume that the sample is of uniform temperature when the sample temperature is measured. In reality, internal temperature gradients are always present when the sample undergoes phase change. This leads then to shifted enthalpy curves depending on a melting or solidification experiment and is known as hysteresis [6, 29].

- For heterogeneous PCMs, the sample size of the experimental method may not be representative [30, 31]. This is important to consider when commercial PCMs are measured, which may contain additives (see next point).

- Many PCMs exhibit so called supercooling [6, 32]. A supercooled state is given when the liquid phase is able to cool down below the phase change temperature. The liquid phase is then in a metastable state instead of solidifying. Once the thermodynamic barrier for solidification is overcome, a part of the liquid phase rapidly solidifies while releasing part of its latent heat (so called recalescence [33]) until the phase change temperature is reached and conventional solidification proceeds. Most of the experimental methods do not account for this phenomenon and have to be simplified [34]. Depending on the material, supercooling may range from just below the solidification temperature down to ambient temperatures. Commercial PCMs usually contain additives to decrease this effect.

To obtain an accurate representation of the PCM properties during phase change is therefore still subject to research. Either by developing new [17, 35] or to standardize existing methods [36].

2.2 Discussion of the T-History Method

In this work, the so called T-History method has been chosen for measuring the enthalpy curve because of its simplicity and suitability for more representative results due to a larger sample size of the method (grams instead of milligrams compared to DSC samples) [6, 37–39]. Larger sample sizes may yield more representative results for commercial PCMs, whose exact composition are unknown, therefore T-History measurements have often been used instead or complementary to DSC measurements in the literature [31, 40].

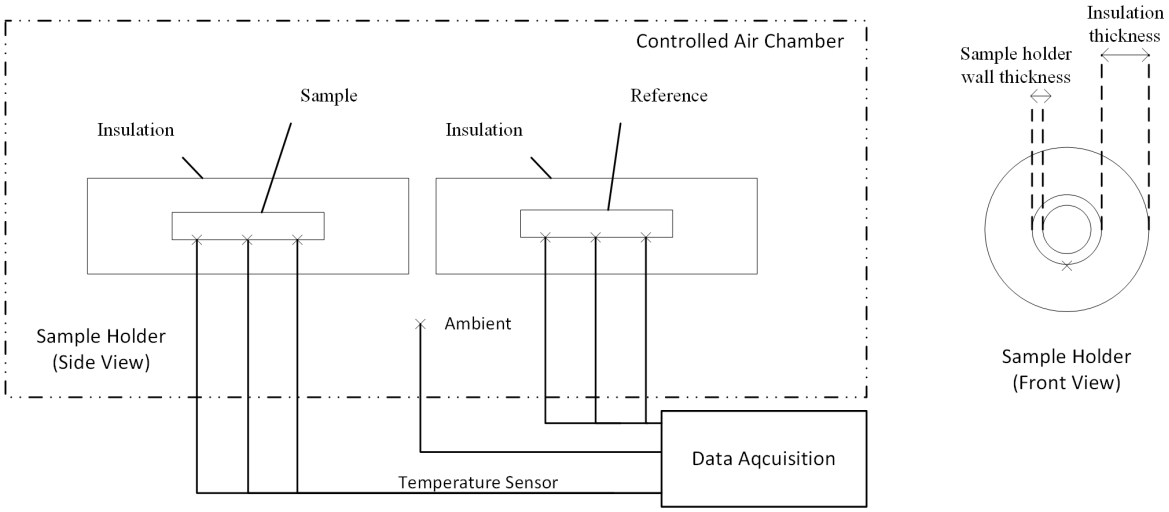

(a)

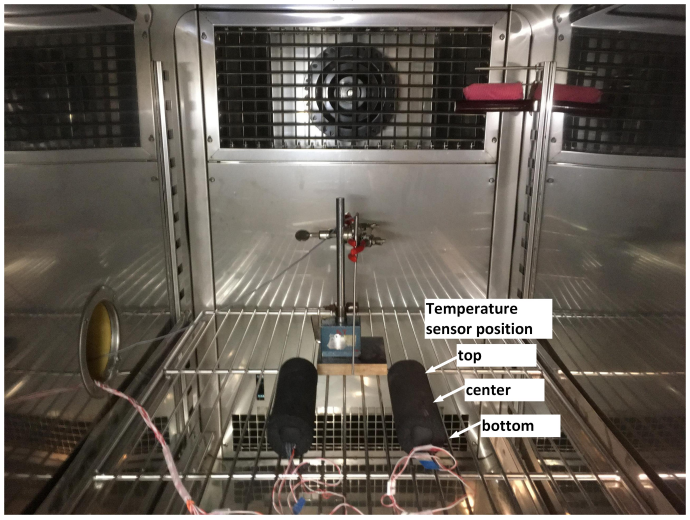

(b)

Figure 2.1: Illustration of the T-History experimental setup (taken from Fig. 2 and 3 of **Paper 2**): (a) Principle sketch and sample holder cross section. Temperature sensor locations are marked by 'x'. (b) Photo of the setup inside the climate chamber. Dimensions of the experimental setup can be found in Tab. 2.1.

The method subjects a sample holder filled with a PCM sample and a reference sample holder with known properties to a step change of the ambient temperature (see Fig. 2.1). The enthalpy curve of the sample is then calculated from the recorded temperature responses of sample and reference (see Fig. 2.2). A separate enthalpy curve is obtained each for solidification and melting.

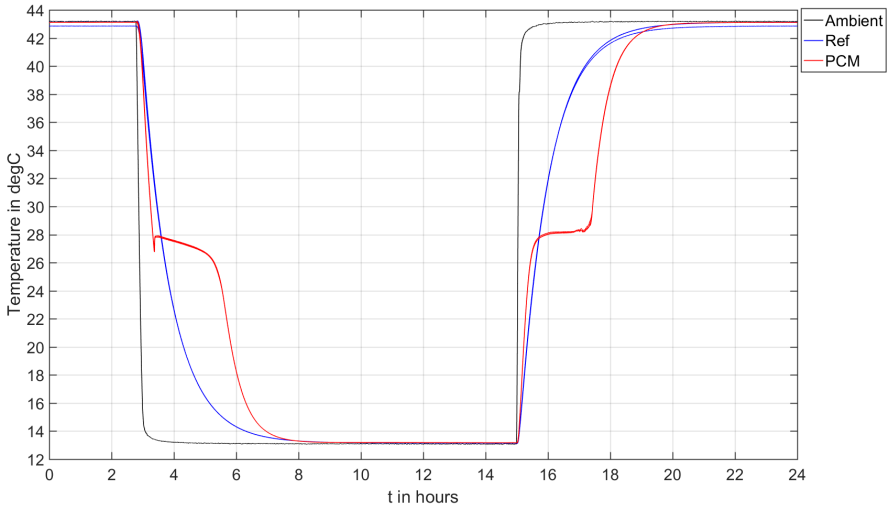

Figure 2.2: Measured temperature response from a PCM sample and reference due to ambient temperature step changes (using the experimental setup given in **Paper 2**). During cooling a small degree of supercooling (ca. 1°C) is visible.

Two main assumptions are made in the method:

1. It is assumed that the overall heat flow between the reference material and the ambient $\dot{Q}_{ref}$, and between the PCM and the ambient $\dot{Q}_{PCM}$, are equal for the same temperature difference $T - T_{amb} = T_{ref} - T_{amb} = T_{PCM} - T_{amb}$ [40]:

$$\dot{Q}_{ref}(T) = \dot{Q}_{PCM}(T) = \frac{1}{R_{th}(T)}(T - T_{amb}) \tag{2.4}$$

   In order to support this assumption in the experiment for three dimensional sample holders containing the PCM and reference, the latter are to be at least of the same geometries, yielding the same effective thermal resistance R_{th} in Eq. 2.4.

2. It is assumed that the measured temperature change over time is representative for the whole sample holder via a lumped model formulation for the sample or reference $k = \{\text{ref}, \text{PCM}\}$ and the sample holder tube:

$$\dot{Q}_k(T) = (m^k \cdot {c_p}^k(T) + m^{tube,k} \cdot {c_p}^{tube}(T)) \cdot \left.\frac{\mathrm{d}T}{\mathrm{d}t}\right|_k \tag{2.5}$$

It is then possible to solve for the unknown effective heat capacity of the PCM ${c_p}^{PCM}(T)$ using the derivatives of the measured temperature responses of sample and reference:

$$ {c_p}^{PCM}(T) = \frac{m^{ref} \cdot {c_p}^{ref}(T) + m^{tube,ref} \cdot {c_p}^{tube}(T)}{m^{PCM}} \cdot \frac{\left.\frac{dT}{dt}\right|_{ref}}{\left.\frac{dT}{dt}\right|_{PCM}} - \frac{m^{tube,PCM} \cdot {c_p}^{tube}(T)}{m^{PCM}} \tag{2.6} $$

For convenience, the terms can be grouped together:
$C_{ref}(T) = \frac{m^{ref} \cdot {c_p}^{ref}(T) + m^{tube,ref} \cdot {c_p}^{tube}(T)}{m^{PCM}}$ and $C_{tube,PCM}(T) = \frac{m^{tube,PCM} \cdot {c_p}^{tube}(T)}{m^{PCM}}$

$$ {c_p}^{PCM}(T) = C_{ref}(T) \cdot \frac{\left.\frac{dT}{dt}\right|_{ref}}{\left.\frac{dT}{dt}\right|_{PCM}} - C_{tube,PCM}(T) \tag{2.7} $$

$$ \Delta h^{PCM} = \int_{T}^{T+\Delta T} {c_p}^{PCM}(\tau) d\tau \tag{2.8} $$

Recent work has shown that the sample holders should be insulated in order for assumption 1 to be valid in an air climate chamber [41]. If the sample holders are uninsulated, the heat transfer is mainly determined by the forced heat transfer coefficient from the sample holder wall to the air, which was shown to be difficult to keep constant and equal for the PCM sample and reference. The insulation serves to dominate the heat transfer (or R_{th}) from sample and reference to the ambient in the experiment via conductive heat transfer through the insulation layer [40, 42]. However, the thermal mass of the insulation is not considered in the method assumptions and its effect on the accuracy of the results not previously studied.

When the representative temperature for PCM and reference is measured at the sample holder wall, assumption 2 should be supported by utilizing a sample holder with low thermal resistance such as copper. Decreasing the overall heating or cooling rate of the experiment (using a thicker insulation or smaller step change of the ambient temperature) will also lead to a smaller temperature gradient during phase change for a given sample holder diameter.

The enthalpy curve obtained from the T-History method can then be used to evaluate the storage potential of a PCM and to estimate its phase change temperature. This information is then used as input to simulate a PCM TES on device level in the next step. In order to improve the method, a discussion on the accuracy and precision of the method was needed. The results of the findings in **Paper 1** and **2** are summarized in the following.

2.2.1 Numerical study of the T-History method

An idealized simulation model in **Paper 1** was used to propagate a known enthalpy curve from a model PCM through the simulated experiment (see Fig. 2.3) in order

to study the validity of the method. The motivation of the paper was to show how well the inserted enthalpy curve (denoted as "true" enthalpy curve) could be reproduced from the simulated temperature versus time curve and the assumptions of the method.

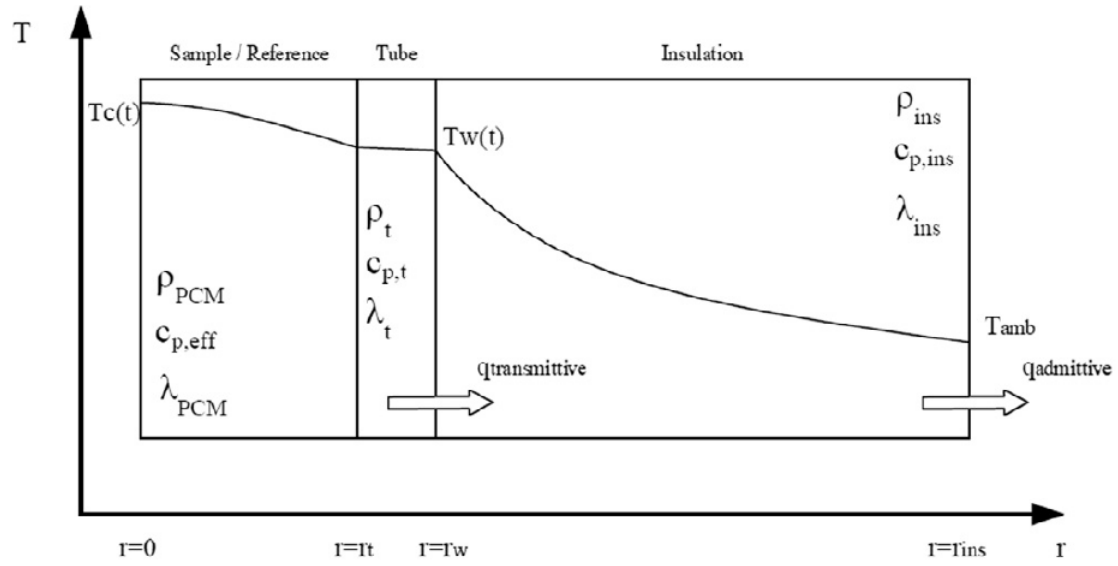

Figure 2.3: Illustration of the simulated T-History experiment (solidification case) and the transmittive and admittive heat fluxes due to the insulation. $\dot{q}_{transmittive}$ is the heat flux density at the measurement sensor position at the sample holder wall (taken from **Paper 1**).

It was found that neglecting the thermal mass of the insulation causes a systematic error in the enthalpy results. The heat flux that is assumed as equal in Eq. 2.4 corresponds to the transmittive heat flux of the insulation at the temperature sensor position and Eq. 2.4 should be more precisely expressed as:

$$\dot{Q}_{ref}^{transmittive}(T) = \dot{Q}_{PCM}^{transmittive}(T) \tag{2.9}$$

This transient heat flux however is not equal while PCM and reference are cooling down or heated up during the experiment. The differences between the two simulated heat fluxes can be observed in Fig. 2.4 and 2.5. The deviations can be summarized as follows:

- The initial transmittive heat fluxes immediately after the temperature step change can deviate considerably, when the PCM and reference have different thermal diffusivities. The temperature evaluation interval should therefore start from a value further from the initial temperature. In **Paper 2** it is shown that the suitable temperature interval is given by a region where $\left.\frac{dT}{dt}\right|_{ref}$ and $\left.\frac{dT}{dt}\right|_{PCM}$ is a linear function of the temperature.

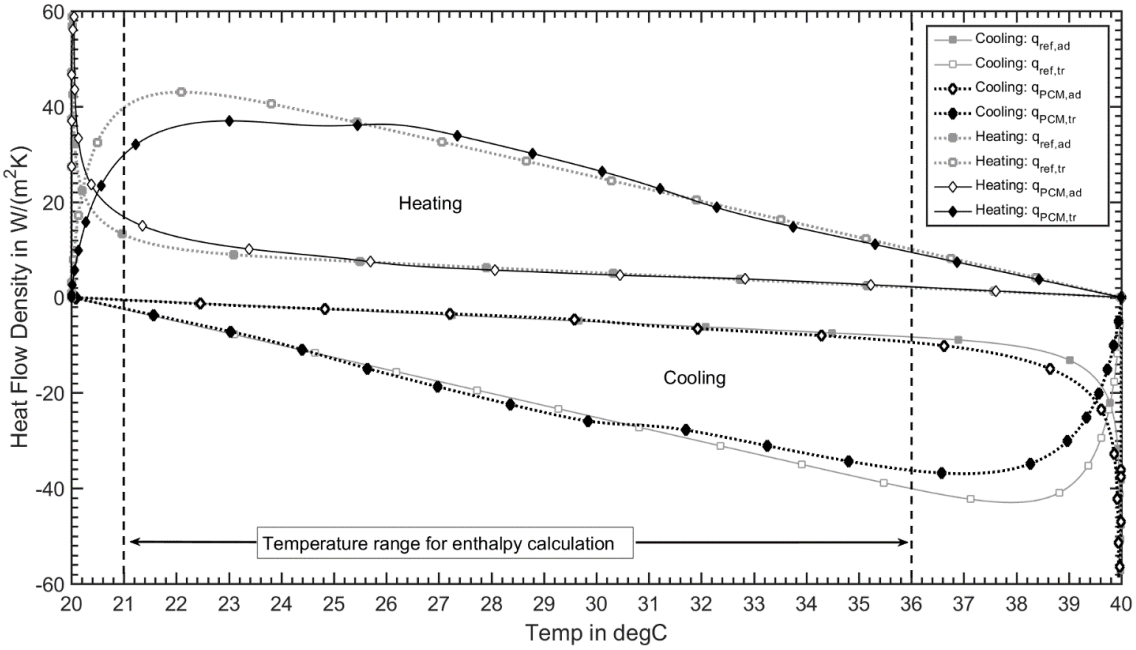

Figure 2.4: Simulated values of $\dot{Q}^{transmittive}$ versus T for PCM and reference (taken from Fig. 7 of **Paper 1**).

- When the PCM undergoes phase change, $\dot{Q}^{transmittive}_{PCM}$ comes close to a steady state heat flux across the insulation with a constant T_{PCM} and T_{amb} at the insulation borders. This near steady state heat flux deviates from $\dot{Q}^{transmittive}_{ref}$ and causes an underestimation of the latent heat portion in the enthalpy results.

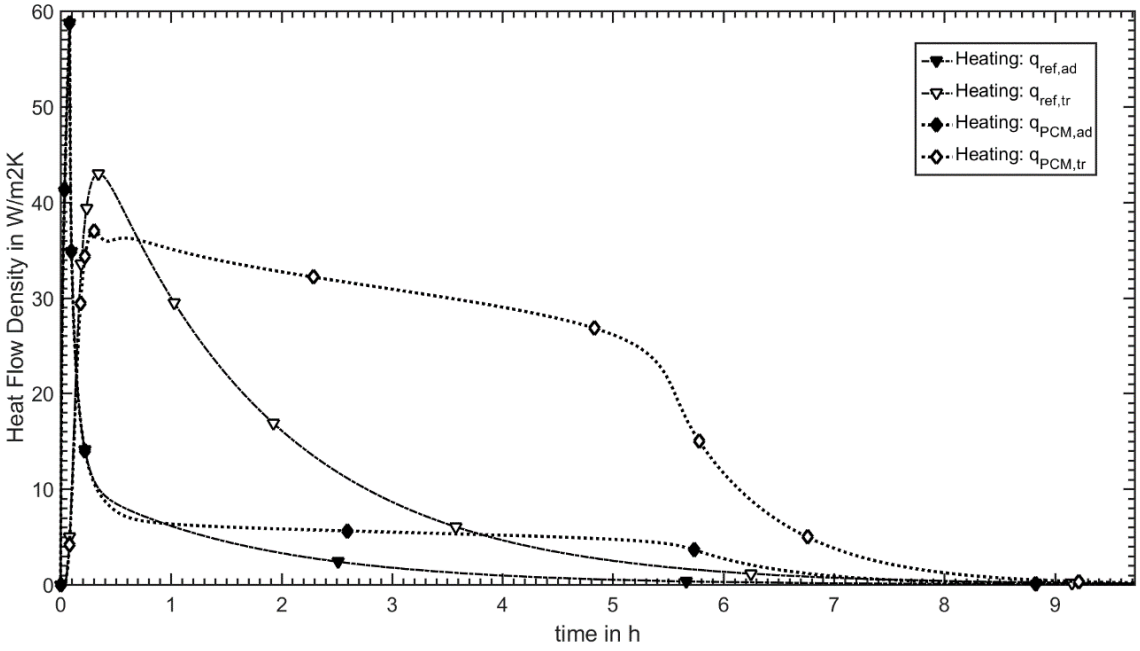

Figure 2.5: Simulated values of $\dot{Q}^{transmittive}$ plotted over time for PCM and reference to illustrate the near steady-state heat flux for the PCM during phase change. (taken from Fig. 9 of **Paper 1**).

Both deviations increase the higher the thermal mass of the insulation is in the experimental setup and a correction of the systematic error should be ideally done.

If the transmittive heat fluxes are known, a temperature dependent correction factor can be calculated and inserted into the original Eq. 2.6:

$$e(T) = \frac{\dot{Q}_{ref}^{transmittive}(T)}{\dot{Q}_{PCM}^{transmittive}(T)} \tag{2.10}$$

$$c_p'^{\,PCM}(T) = C_{ref}(T) \cdot \frac{1}{e(T)} \frac{\left.\frac{dT}{dt}\right|_{ref}}{\left.\frac{dT}{dt}\right|_{PCM}} - C_{tube,PCM}(T) \tag{2.11}$$

However, if the heat fluxes are not known, since only the temperature is usually measured, it may be enough to use a steady state assumption close to the phase change temperature instead of Eq. 2.10:

$$e^{simplified} = \frac{\dot{Q}_{ref}^{transmittive}(T_{PCM})}{\dot{Q}_{ref}^{steady-state}(T_{PCM})} = \text{const.} \tag{2.12}$$

As shown in Fig. 2.6, it was possible to correct the overall enthalpy underestimation with both approaches.

Within the parameters of the numerical study, the relative error was quantified as around 1 to 4 % for the chosen enthalpy difference. It was then concluded, that this predicted systematic error has to be verified and studied experimentally, to place it in relation with other factors influencing the obtained enthalpy results.

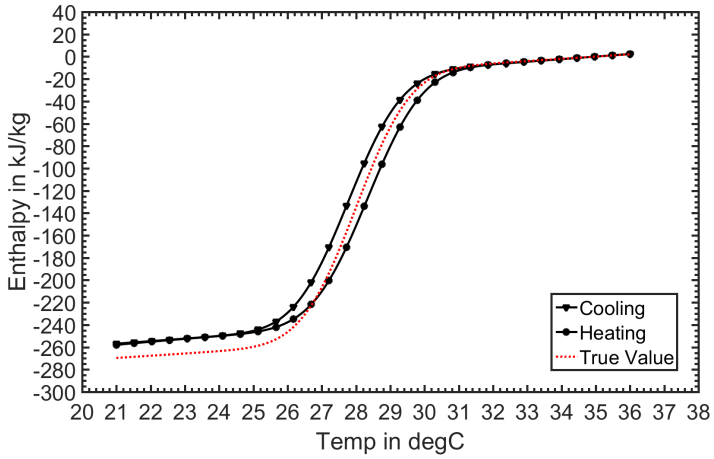

(a)

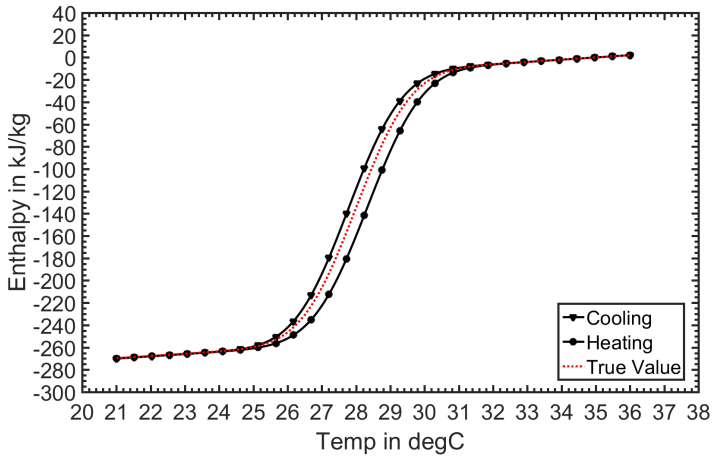

(b)

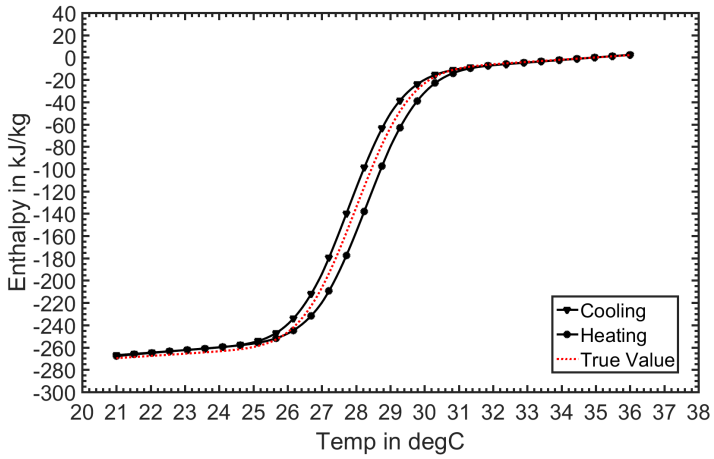

(c)

Figure 2.6: Example of obtained enthalpy results due to the neglected sample holder insulation (taken from Fig. 5, 12 and 16 of **Paper 1**). (a): Uncorrected heat flux. (b): Using a temperature dependent correction factor (Eq. 2.10). (c): Using a steady state assumption (Eq. 2.12).

2.2.2 Experimental study of the T-History method

In **Paper 2** a systematic experimental study has been conducted on a commercial PCM using different sample holder sizes and insulation thicknesses (see Tab. 2.1) in order to reveal any present systematic errors as discussed previously.

Table 2.1: Sample holder properties used in the experimental study of **Paper 2**. For setup B1 and B2 the same 15mm sample holder is used but with different insulation types.

Parameter	Setup A	Setup B1	Setup B2	
Sample holder (outer) diameter	10	15	15	mm
Insulation thickness	15.5	17	32	mm
m^{PCM} (RT28HC, paraffin)	4.2	10.1	10.1	g
m^{ref} (distilled water)	5.4	13.1	13.1	g
$m^{tube,PCM}$	25.2	46.8	46.8	g
$m^{tube,ref}$	25.0	46.9	46.9	g

When calculating the enthalpy values, it was found that the temperature over time derivatives $\frac{dT}{dt}\Big|_{ref}$ and $\frac{dT}{dt}\Big|_{PCM}$ in Eq. 2.6 have to be cleared from noise in order not to under- or overestimate the effective heat capacity of the PCM when using real experimental data. This is especially important because any noise in the original data is further enhanced when forming the derivative [43, 44]. Moreover, the period during recalescence, when the PCM rapidly solidifies from its supercooled state, is assumed to be adiabatic in order to avoid negative heat capacity values in Eq. 2.6. Details of the exact data processing procedure are outlined in **Paper 2**.

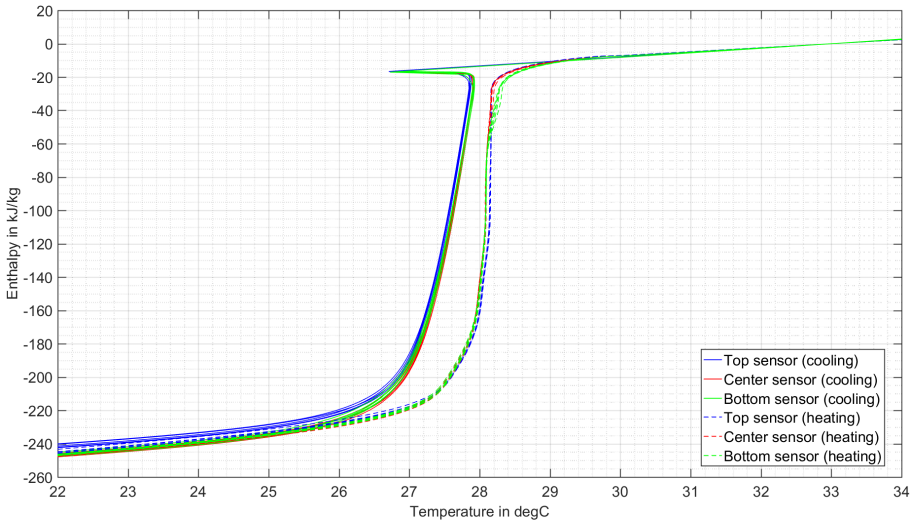

Figure 2.7: Enthalpy versus temperature curves for the Setup B2-I of **Paper 2** (taken from Fig. 19 of **Paper 2**).

From the obtained enthalpy results shown in Fig. 2.7 and 2.8 it can be concluded that de-noising the data improves the precision of the method and repeatable results

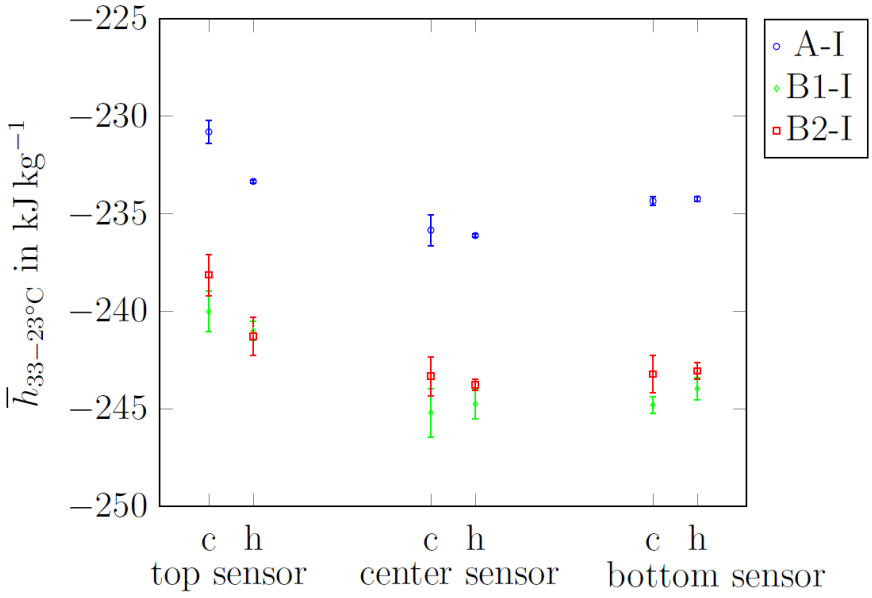

Figure 2.8: Mean enthalpy results and standard deviation for Setup A-I, B1-I and B2-I over five cycles for each sensor location (c: cooling, h: heating) (taken from Fig. 15 of **Paper 2**).

are obtained for all setups. The results are however shifted to smaller enthalpy values the higher the thermal mass of the insulation is with respect to the sample holder thermal mass as predicted in **Paper 1**.

Monte Carlo simulations have moreover been used in order to study the effect of propagating uncertainties of all input quantities in Eq. 2.6 on the enthalpy results (see Fig. 2.9). Each input quantity, such as the sample and reference mass, is assigned a probability density function and a number is drawn randomly from the distribution to calculate the enthalpy curve for each Monte Carlo trial. A high enough number of Monte Carlo trials allows then an estimation of the probability density function of the enthalpy value [45].

It can be concluded that the larger sample holders of setup B1 and B2 are preferable since a larger absolute value in e.g. mass of sample and sample holder tube dampen the effect of uncertainties compared to the smaller sample holder.

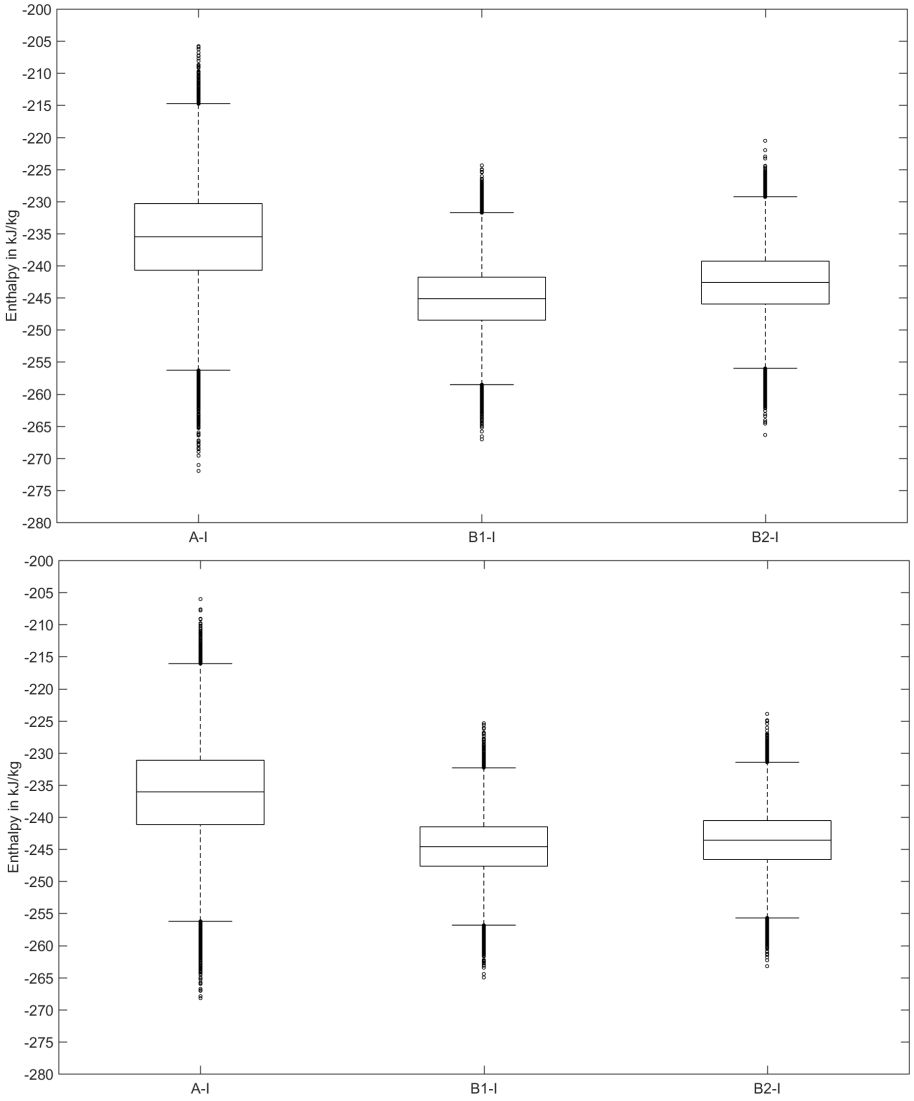

Figure 2.9: Example of spread of $\Delta h_{33-23^{\circ}\mathrm{C}}$ values obtained from 100000 Monte Carlo simulations by propagating uncertainties of setup input quantities through the mathematical model: (a): cooling, (b): heating (taken from Fig. 26 and 27 of **Paper 2**)

2.3 Generation of PCM proxy models

The measured enthalpy curves using the data evaluation and experimental setup from **Paper 2** can then be used to generate proxy PCM models. The latter are then representative for the melting and solidification behavior of the material on device scale.

A simple way of representing the phase change, as an alternative to the effective heat capacity method, is to model the latent heat using a liquid fraction term g. The latter can be represented by a functional relationship with the temperature $g = F(T)$. Following [46], g is assumed to be linear:

$$g = F(T) = \begin{cases} 0 & T \leq T_S, \text{ fully solid} \\ \frac{T - T_S}{T_L - T_S} & T_S < T < T_L, \text{ transition state} \\ 1 & T \geq T_L, \text{ fully liquid} \end{cases} \tag{2.13}$$

When a PCM is known to change phase almost isothermally at T_{PCM}, the solidus and liquidus temperature can be specified using a very small temperature difference $w \to 0$: $T_S = T_{PCM} - \frac{w}{2}$, $T_L = T_{PCM} + \frac{w}{2}$.

Compared to modeling a PCM with an effective heat capacity, this has the benefit of avoiding cases like $c_p^{PCM} \to +\infty$ for near isothermal phase change.

Material properties that are dependent on the liquid and solid phases, such as the specific heat capacity in the sensible regions, can also be accounted for using the liquid fraction:

$$c_p = (1 - g)\ c_p^S + g\ c_p^L \tag{2.14}$$

The enthalpy change can then be expressed using a sensible and latent heat term:

$$\Delta h_{1-2} = \int_{T_1}^{T_2} c_p(T) \mathrm{d}T + \int_{T_1}^{T_2} \frac{\mathrm{d}F(T)}{\mathrm{d}T} L\ \mathrm{d}T \tag{2.15}$$

Fig. 2.10 shows the approach using the T-History enthalpy curves from a commercial PCM (RT10HC) that melts approximately between 9.5 to 10 °C. This PCM is considered for the TES design case in later chapters.

Table 2.2: Proxy model parameters for RT10HC used in Fig. 2.10.

	F1	F2	F3	
T_{PCM}	9.6	9.45	9.75	°C
(same for F1-F3)		w	0.5	°C
		L	145	$\mathrm{kJ\,kg^{-1}}$
		c_p^S	4600	$\mathrm{J\,kg^{-1}\,K^{-1}}$
		c_p^L	2600	$\mathrm{J\,kg^{-1}\,K^{-1}}$

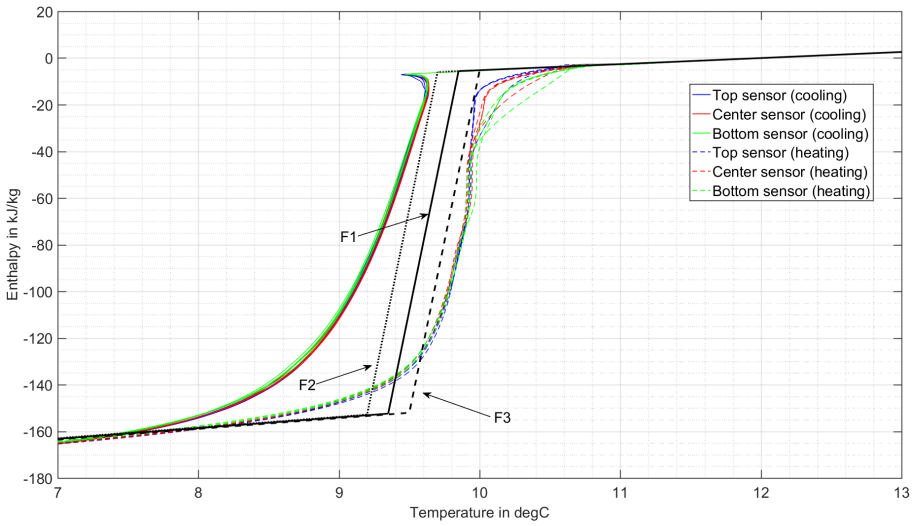

Figure 2.10: Enthalpy versus temperature curve of the commercial PCM RT10HC using the experimental setup B2 from **Paper 2**. F1 to F3 correspond to three different proxy models (see Tab. 2.2).

2.4 Conclusions & Outlook for the T-History method

In the previous sections, the validity of the T-History method has been discussed based on numerical and experimental studies. It was shown that the current mathematical model leads to systematic errors in the enthalpy results. Moreover, it was shown that data processing algorithms are necessary to avoid wrong representations of the results due to noise. The proposed setup and data algorithm from **Paper 2** however allows repeatable measurement results (consistent for both melting and solidification) and a small hysteresis, which can be seen as an contribution to the method. Due to the revealed systematic errors, it is recommended to compare the obtained values with other sources whenever available. This recommendation can be made for any measurement method, until validated measurement standards have been defined.

In future work, the proposed correction method from **Paper 1** may be applied on real experiments in order to reduce any existing systematic errors further. Any further improvements in the material characterization method will also lead to more accurate PCM proxy models, which in turn increase the accuracy of any simulation models involving PCMs.

Chapter 3

PCM TES Model development

3.1 Model Description

In the following, a PCM TES model for the geometries previously shown in Fig. 1.5 is presented. The model is used to estimate the performance for (dis)charging the PCM TES by simulating the heat transfer between a HTF and PCM for melting and solidification of the latter.

The rectangular and cylindrical geometry can be seen as an approximation for plate or shell and tube heat exchanger configurations, respectively. It is assumed that each TES consists of a number of identical channels ($N_{channel}$) containing PCM, a heat transfer WALL and the HTF. Fig. 3.1 and 3.2 show one channel and the possible simplifications assuming symmetry lines for each geometry.

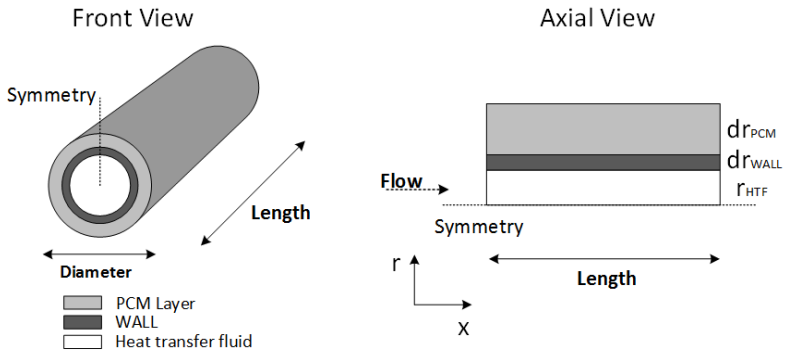

Figure 3.1: Illustration of the simulated domain for the cylindrical geometry. Rotational symmetry is assumed.

The model shown in this thesis was developed in response to the recent work done by Pointner et al. 2016 [47], who compared different modeling methods of phase change materials. Among them, the so called source term method (based on the work of Voller & Swaminathan 1991 [46]) implemented in a finite volume method (FVM) model in `MATLAB` yielded competitive computation times for solving phase change problems, while retaining a comparable solution to commercial CFD software. In the following, the principle of combining the source term method with a FVM model and applied to the above geometries is described in detail.

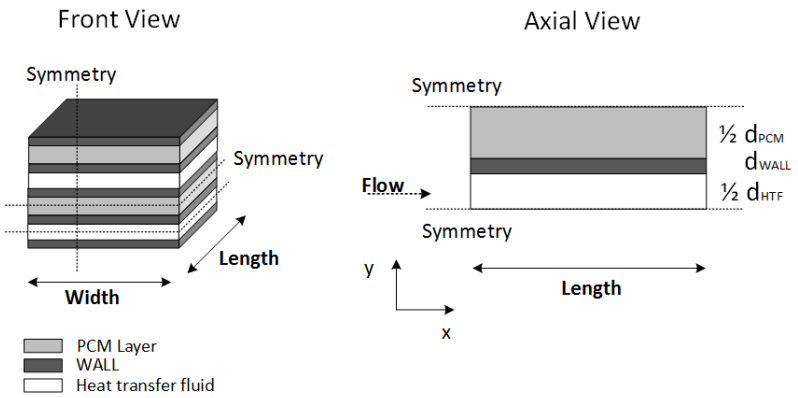

Figure 3.2: Illustration of the simulated domain for the rectangular geometry. Symmetry for the width as well as for half of the HTF and PCM domain height is assumed.

For each computational node, an energy balance equation is formulated considering a convection-, diffusion- and source term [48]:

$$\frac{\partial h}{\partial t} = -\boldsymbol{\nabla} \cdot (h\boldsymbol{u}) - \boldsymbol{\nabla} \cdot \dot{\boldsymbol{q}} + S \tag{3.1}$$

or in tensor notation:

$$\frac{\partial h}{\partial t} = -\frac{\partial}{\partial x_j}(hu_j) - \frac{\partial}{\partial x_j}\dot{q}_j + S \tag{3.2}$$

The specific enthalpy h ($\mathrm{J\,m^{-3}}$) in Eq. 3.1 is formulated with respect to the node volume.

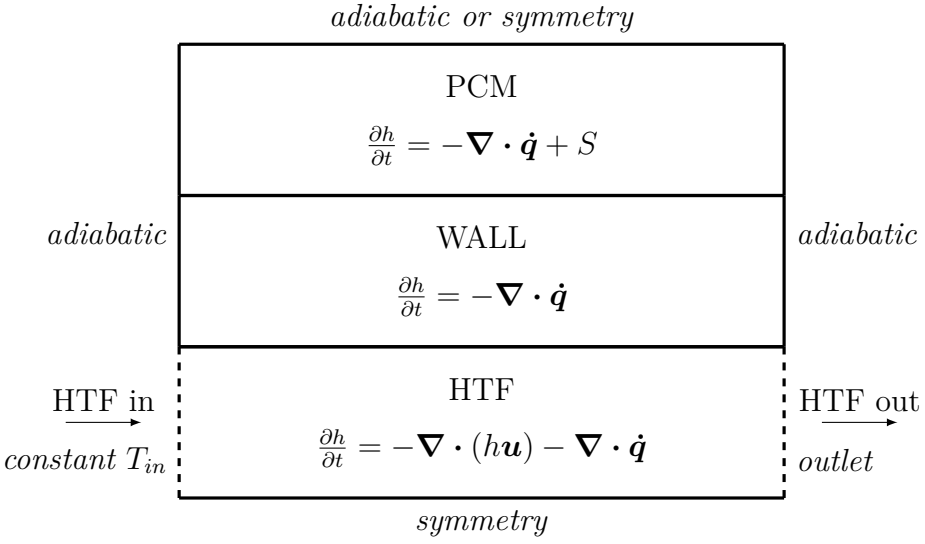

Figure 3.3: Overview of balance equations and boundary conditions for the simulated two-dimensional domain (axial view corresponding to Fig. 3.1-3.2).

The storage model is split up into a heat transfer fluid (HTF), wall (WALL) and phase change material (PCM) sub-domain according to Fig. 3.3 and considers the following simplifications of Eq. 3.1:

- HTF: The velocity profile is prescribed and considered as fully developed. No momentum balance equation is solved.
- WALL & PCM: Only heat conduction is considered. The latent heat in the PCM domain is accounted for as a sink or source term depending on melting or solidification, respectively.

The FVM applies the Gaussian Divergence Theorem over each node control volume. This simplifies the energy balance for every node to the incoming or outgoing convective and conductive heat fluxes across the node faces:

$$\int_{c.v.} \frac{\partial h}{\partial t} \, \mathrm{d}V = -\int_{c.v.} \boldsymbol{\nabla} \cdot (h\boldsymbol{u}) \, \mathrm{d}V - \int_{c.v.} \boldsymbol{\nabla} \cdot \dot{\boldsymbol{q}} \, \mathrm{d}V + \int_{c.v.} S \mathrm{d}V \tag{3.3a}$$

$$\int_{c.v.} \frac{\partial h}{\partial t} \, \mathrm{d}V = -\oiint_{S} h\boldsymbol{u} \, \mathbf{d}\boldsymbol{S} - \oiint_{S} \dot{\boldsymbol{q}} \, \mathbf{d}\boldsymbol{S} + \int_{c.v.} S \mathrm{d}V \tag{3.3b}$$

For each node P, the fluxes across the faces can be formulated using the differences in temperatures from the neighboring node (nb) N, E, S, W and the node widths Δx, Δz following a node centered discretization according to Fig. 3.4. This then leads to a coefficient form of the balance equation for each node:

$$a_P T_P = \sum_{nb} a_{nb} T_{nb} + b_P T_P^0 + \rho_P L_P (g_P^0 - g_P) \tag{3.4}$$

The FVM coefficients a_i follow from the discretization schemes for the fluxes and the modeled geometry. Only structured meshes are considered in this work as the nodes are assumed to be equidistant in axial direction for the whole domain and equidistant in orthogonal direction within each material domain (see Fig. 3.5).

- The transient terms are formulated using a fully implicit scheme, that is the complete temperature field depends on the current to be solved time step.
- The source term $\rho_P L_P (g_P^0 - g_P)$ in Eq. 3.4, representing the latent heat released or stored by a PCM node in a time step, is formulated using updates of a liquid fraction g. The latter is given by a functional relationship with the node temperature: $g = F(T)$ as described in Chapter 2.3.
- The conduction fluxes are approximated using a central difference scheme [48]. Across nodes, the harmonic mean of thermal conductivities is calculated when formulating the conductive heat flux in order to account for a consistent heat flux across material boundaries [49].

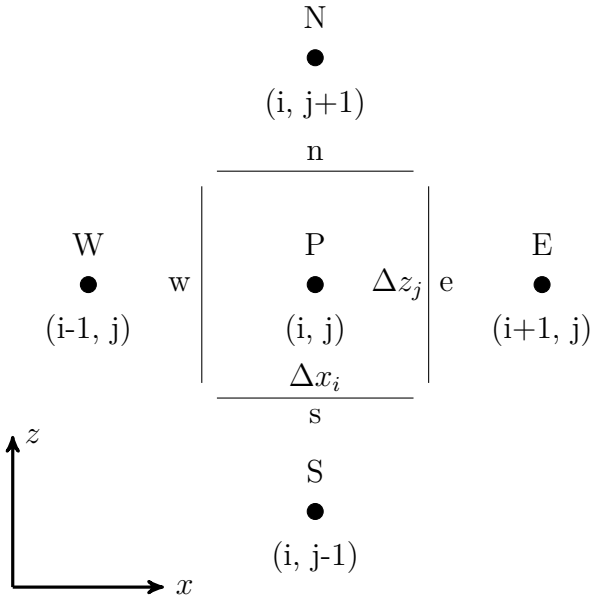

Figure 3.4: Sketch of a node centered mesh with node centers and faces given in compass notation (P, N, E, S, W) and (n, e, s, w), respectively. Node faces are located between two adjacent node centers depending on the node dimensions (e.g. $w = (i - \frac{1}{2}\Delta x_i, j)$ and $e = (i + \frac{1}{2}\Delta x_i, j)$). The orthogonal coordinate z is representative for r or y for a cylindrical or rectangular case, respectively.

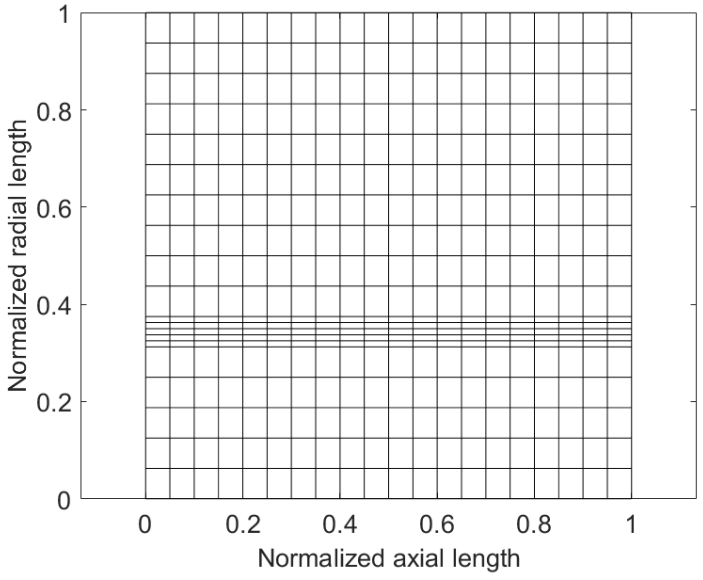

Figure 3.5: Illustration of a structured FVM mesh with $N = 400$ nodes (20 axial nodes, 5 radial nodes for HTF, 5 nodes for WALL and 10 nodes for PCM sections).

- The convection flux is approximated using a first order upwind formulation [48]. A parabolic velocity profile is given for both geometries from the average

channel velocity $u_{channel}$ and the maximum domain height:

For pipes:

$$u(r) = u_{max}\left(1 - \frac{r^2}{r_{max}^2}\right) = 2u_{channel}\left(1 - \frac{r^2}{r_{max}^2}\right) \tag{3.5}$$

For rectangular channels (parallel plates):

$$u(y) = u_{max}\left(1 - \frac{y^2}{y_{max}^2}\right) = 1.5u_{channel}\left(1 - \frac{y^2}{y_{max}^2}\right) \tag{3.6}$$

- Forced convection heat transfer between the HTF and WALL is represented using a Nusselt number correlation. The velocity and temperature fields are assumed to be fully developed. For laminar flow and assuming a constant temperature boundary condition, the Nusselt number for a pipe is then given in [50] as:

$$\mathrm{Nu} = \frac{L_{ch} h_{WALL}}{\lambda_{HTF}} = 3.66 \tag{3.7}$$

  The value for the heat transfer coefficient h_{WALL} is therefore a function of the characteristic length of the HTF channel and is assumed as constant along the axial length.

- Perfect thermal contact is considered for the WALL and PCM interface at this stage of the project due to lack of further information [19].

The discretization schemes are well documented in standard FVM literature such as [48, 49] and not repeated explicitly in this work. Eq. 3.4 formulated for all nodes can then be summarized as a system of linear equations. The equation system is then solved for the unknown temperature field $\boldsymbol{T}$ for each time step:

$$\boldsymbol{A} \cdot \boldsymbol{T} = \boldsymbol{b} \tag{3.8}$$

Updates for the liquid fraction have to be done manually for m iterations within each time step until the temperature $\boldsymbol{T}$ and liquid fraction fields $\boldsymbol{g}$ are consistent for all PCM nodes following their coupling via Eq. 2.13. The formulation via a Taylor series given in [46] is used to update the liquid fraction field from the temperature field solution after solving Eq. 3.8.

$$\boldsymbol{g^{m+1}} = \boldsymbol{g^{m}} + \alpha \frac{\mathrm{d}F}{\mathrm{d}T}\left[\boldsymbol{T^{m+1}} - F^{-1}(\boldsymbol{g^{m}})\right] \tag{3.9}$$

When formulating the model it was found that an under-relaxation factor α in Eq. 3.9 is necessary to prevent a computational node changing from $g^m = 0$ to $g^{m+1} = 1$ within one iteration. The latter case would lead to numerical instabilities for larger time steps as the source/sink term would then be severely overestimated. A value of $\alpha = 0.1$ ensured stable updates of the liquid fraction for all simulated cases in this work.

Convergence within one time step is declared when the largest relative enthalpy deviation among all nodes is smaller than a specified tolerance [46]:

$$\epsilon = \max\left|\frac{\boldsymbol{H^{m+1}} - \boldsymbol{H^{m}}}{\boldsymbol{H^{m}}}\right| < 10^{-3} \tag{3.10}$$

The whole solving procedure is summarized in Fig. 3.6.

```
   /* Load initial conditions t = t_0                                          */
 1 let T^0 := T(t = t_0) ;                                  // Temperature field
 2 let g^0 := g(t = t_0) ;                                  // Liquid fraction field
   /* Calculate for each time step                                             */
 3 for t ← t_0 to t_end by Δt do
       /* Update liquid fractions within each time step                       */
 4     let it_m := 1 ;                  // count iterations within a new time step
 5     repeat
 6         if it_m = 1 then
               /* First iteration starts with values from previous time step  */
 7             let T^m := T^0;
 8             let g^m := g^0;
 9         else
               /* Higher iterations start with values from previous iteration */
10             let T^m := T^{m+1};
11             let g^m := g^{m+1};
12         end
13         Calculate coefficient matrix A and right hand side vector b from g^m and T^0 ;
           /* Solve temperature field A · T^{m+1} = b                         */
14         T^{m+1} = A\b ;                                  // MATLAB's mldivide
           /* Update liquid fraction field                                    */
15         g^{m+1} = g^m + α dF/dT [T^{m+1} − F^{-1}(g^m)] ;
           /* Over- and undershoot correction                                 */
16         if g^{m+1} > 1 then
17             let g^{m+1} := 1;
18         else if g^{m+1} < 0 then
19             let g^{m+1} := 0;
           /* Check if temperature and liquid fraction are consistent for all
              nodes by calculating the largest enthalpy deviation.            */
20         ε = max| (H^{m+1} − H^m) / H^m | ;
21         let it_m := it_m + 1 ;
22     until ε < ε^{max} = 10^{-3};
       /* Assign last iteration to current time step                          */
23     let T(t) := T^{m+1} ;
24     let g(t) := g^{m+1} ;
       /* Assign current time step as start values for next time step         */
25     let T^0 := T(t) ;
26     let g^0 := g(t) ;
27 end
```

Figure 3.6: Pseudo code to illustrate the liquid fraction update within each time step given by Voller 1991 [46]. In this work an under-relaxation factor $0 < \alpha < 1$ is included (line 15) in order to prevent a computational node changing from $g^m = 0$ to $g^{m+1} = 1$ within one iteration.

3.2 Comparison with a literature model

At this stage of the project, the model can be seen as not experimentally verified. However, the model performance can be evaluated in terms of a global energy balance and the consistency of mesh and time step refinements [48]. Moreover, it can be compared to existing literature models.

The study done by Lacroix 1993 [56] is chosen for comparison, since it has often been used as reference when own experimental results are not available [20].

The study is restricted to the cylindrical geometry of Fig. 3.1, where a single copper tube with water as HTF is surrounded by a PCM layer (n-octadecane as PCM). The thickness of the PCM layer is varied for two cases. The channel is initially at a temperature -10K below the PCM melting temperature. A HTF with a temperature of $+5$ to $+20$K above the melting temperature and different mass flow rates is then supplied for 3600 s to melt the PCM and the HTF outlet temperature variations are obtained from the model. All parameters used to simulate 18 different cases are listed in Tab. 3.1 and 3.3. It is noted however, that the cases can not be reproduced exactly because not all material data is provided in the paper. Main differences between the model in this work and the literature model are summarized as:

- Lacroix 1993 uses the same source term method with a finite difference approach instead of the FVM.
- Lacroix 1993 includes an empirical equation to calculate an effective thermal conductivity for the PCM liquid phase to indirectly account for natural convection. This is not done in the model of this thesis.
- The heat transfer resistance of the copper tube is neglected in Lacroix 1993 but included in this model.
- The Nusselt number is calculated as a function of the axial length in the literature model, while it is assumed as constant in this model.

Table 3.1: Material parameters used in Lacroix 1993 and this work.

	Lacroix	This work	Unit	Comment
T_{PCM}	300.7	same	K	
T_S	n/a	300.65	K	
T_L	n/a	300.75	K	
L	243.5	same	$\mathrm{kJ\,kg^{-1}}$	
λ_S^{PCM}	0.358	same	$\mathrm{W\,m^{-1}\,K^{-1}}$	
λ_L^{PCM}	0.148	same	$\mathrm{W\,m^{-1}\,K^{-1}}$	
c_p^{PCM}	n/a	2000	$\mathrm{J\,kg^{-1}\,K^{-1}}$	estimated for n-octadecane [57]
ρ^{PCM}	n/a	836.4	$\mathrm{kg\,m^{-3}}$	calculated from solid thermal diffusivity value [56].
λ^{WALL}	neglected	300	$\mathrm{W\,m^{-1}\,K^{-1}}$	estimated for copper [57]
c_p^{WALL}	neglected	385	$\mathrm{J\,kg^{-1}\,K^{-1}}$	estimated for copper [57]
ρ^{WALL}	neglected	8900	$\mathrm{kg\,m^{-3}}$	estimated for copper [57]
λ^{HTF}	n/a	0.6	$\mathrm{W\,m^{-1}\,K^{-1}}$	estimated for water [50]
c_p^{HTF}	n/a	4180	$\mathrm{J\,kg^{-1}\,K^{-1}}$	estimated for water [50]
ρ^{HTF}	n/a	1000	$\mathrm{kg\,m^{-3}}$	estimated for water [50]

Table 3.2: Simulation parameters used in Lacroix 1993 and this work. The radial thickness dr_i corresponds to Fig. 3.1.

Case independent parameters	Value	Unit	Comment
T^0	$T_{PCM} - 10$	K	
T_{in}	$T_{PCM} + \Delta T$	K	ΔT varied in Tab. 3.3
Axial length	1	m	
r_{HTF}	6.35	mm	
dr_{WALL}	1.55	mm	Heat transfer resistance of the wall is neglected in Lacroix 1993.
h_{WALL}	172.91	$\mathrm{W\,m^{-2}\,K^{-1}}$	In Lacroix 1993 a non constant Nusselt number is used along the axial length.

Table 3.3: Simulated cases by Lacroix 1993 and this work. The radial thickness dr_i corresponds to Fig. 3.1. ΔT corresponds to the inlet temperature $T_{in} = T_{PCM} + \Delta T$.

dr_{PCM} in mm	Tag 1	$\dot{m}$ in $\mathrm{kg\,s^{-1}}$	Tag 2	ΔT in K	Tag 3	t_{end} in s	Tag 4
3.1	a	1.5×10^{-4}	1	5	1	3600	1
10.4	c	1.5×10^{-3}	2	10	2		
		1.5×10^{-2}	3	20	3		

3.2.1 Global Energy Balance

The correctness of the solution can be first checked by means of a global energy balance. In each time step the difference of the energy going in and out of the system at the HTF in- and outlet (see Fig. 3.3) should be equal to the energy increase or decrease of the whole domain (sum over all nodes N) depending on a melting or solidification case, respectively: $\Delta Q^{boundaries}(\Delta t) = \Delta Q^{domain}(\Delta t)$.

$$\Delta Q^{boundaries}(\Delta t) = \dot{m}^{HTF} c_p^{HTF} (T_{in} - \Delta T_{out}(\Delta t))\ \Delta t \tag{3.11}$$

$$\Delta Q^{domain}(\Delta t) = \sum_i^N \left[V^i \left(\rho^i c_p^i \Delta T^i(\Delta t) + \rho^i L^i \Delta g^i(\Delta t) \right) \right] \tag{3.12}$$

This is exemplary shown for the case *a231*, where the complete domain from the initial temperature T^0 reaches steady state with the HTF inlet temperature T_{in} ($\Delta T_{max} = 20$K) (visible by the constant HTF outlet temperature in Fig. 3.15).

The total energy necessary for this can be calculated before the simulation since the heat capacities of HTF, WALL and PCM as well as the volume of each material section are known:

$$\Delta Q_{tot} = 1.94 \times 10^{-2}\ \text{kWh} \tag{3.13}$$

The cumulated energy across the boundaries and of all nodes is shown in Fig. 3.7 for a mesh with 32000 nodes and a simulated time step of 1s. It can be seen that they are consistent with the previously calculated value. Moreover, the relative error between the cumulated energy change between boundary and domain are shown in Fig. 3.8. It can be seen that the largest error is due to the first time step and becomes negligible the longer the simulation progresses. The error does not increase significantly with a larger time step or a much coarser mesh (see. Fig. 3.9).

It can therefore be concluded that both the specified tolerance for temperature and liquid fraction updates in Fig. 3.6 and the solution of the linear equation solver for each time step is accurate enough for the considered mesh and time steps.

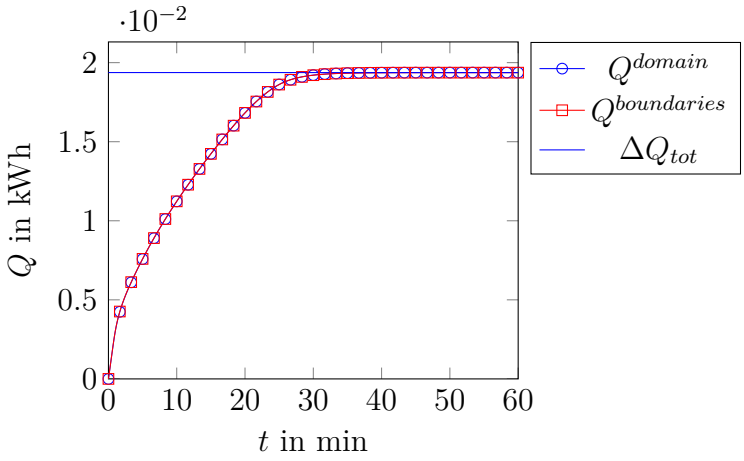

Figure 3.7: Cumulated energy change of HTF boundary and domain over the simulated time for case *a231* and a fine mesh: $N = 32000$, $\Delta t = 1$s.

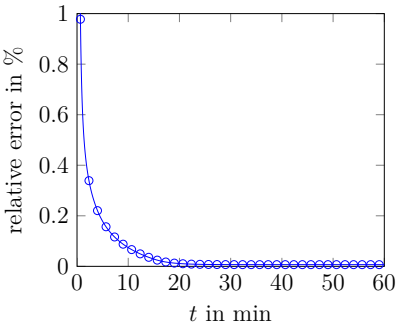

Figure 3.8: Relative error between cumulated energy change of HTF boundary and domain over the simulated time for case *a231* and a fine mesh: $N = 32000$, $\Delta t = 1$s.

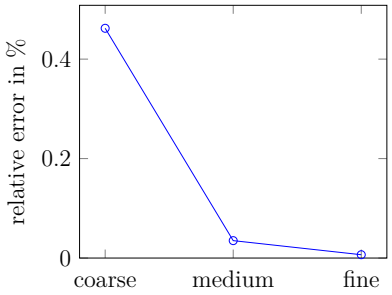

Figure 3.9: Relative error at $t = 3600$s between cumulated energy change of HTF boundary and domain for different mesh sizes and time steps for case *a231*. Coarse: $N = 9600$, $\Delta t = 5$s; Medium: $N = 17200$, $\Delta t = 1$s; Fine: $N = 32000$, $\Delta t = 1$s

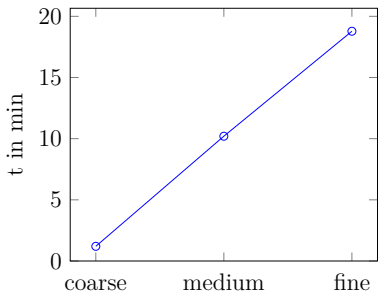

Figure 3.10: Computation time (64bit Windows 7 laptop, Intel i7-5600 2.6GHz CPU, 16GB RAM) for different mesh sizes and time steps for case *a231*. Coarse: $N = 9600$, $\Delta t = 5$s; Medium: $N = 17200$, $\Delta t = 1$s; Fine: $N = 32000$, $\Delta t = 1$s

3.2.2 Comparison with simulated cases from Lacroix 1993

In the following, all simulation cases from Tab. 3.3 are presented using the medium mesh of $N = 17200$ nodes and a time step of $\Delta t = 1$s. From the evolution of the HTF outlet temperature shown in Fig. 3.11 to 3.16 it can be seen that the model in this work is comparable to the literature model for all studied cases. The agreement however appears to be better for the low mass flow rate cases (*a1xx* and *c1xx*). The deviations at higher mass flow rates are then likely due to the different assumptions in the model, such as using a different forced heat transfer coefficient at the wall and/or not including an empirical correlation for convective melting.

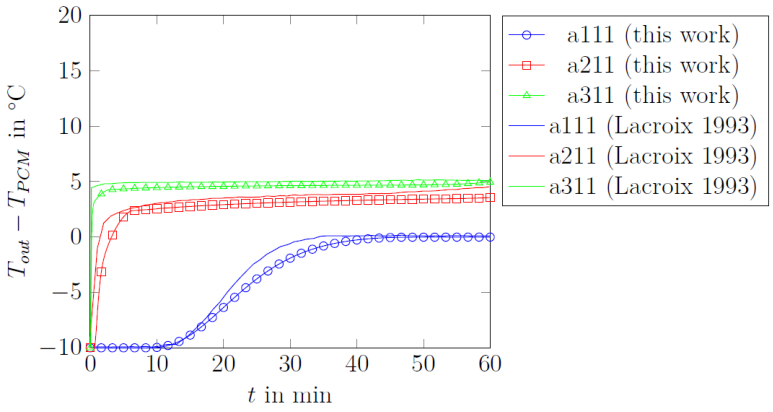

Figure 3.11: Comparison of simulated HTF outlet temperatures with $\Delta T = 5$K and $dr_{PCM} = 3.1$mm for different mass flow rates (see Tab. 3.3).

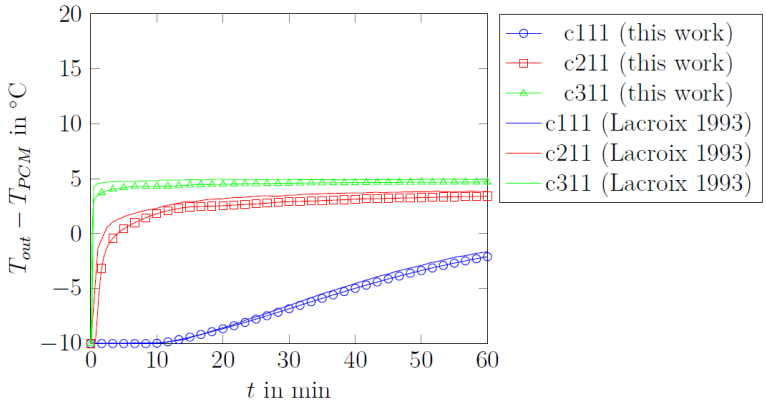

Figure 3.12: Comparison of simulated HTF outlet temperature with $\Delta T = 5$K and $dr_{PCM} = 10.4$mm for different mass flow rates (see Tab. 3.3).

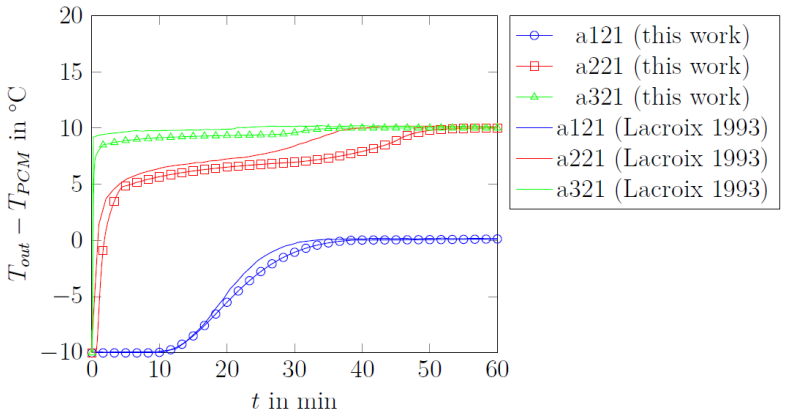

Figure 3.13: Comparison of simulated HTF outlet temperature with $\Delta T = 10$K and $dr_{PCM} = 3.1$mm for different mass flow rates (see Tab. 3.3).

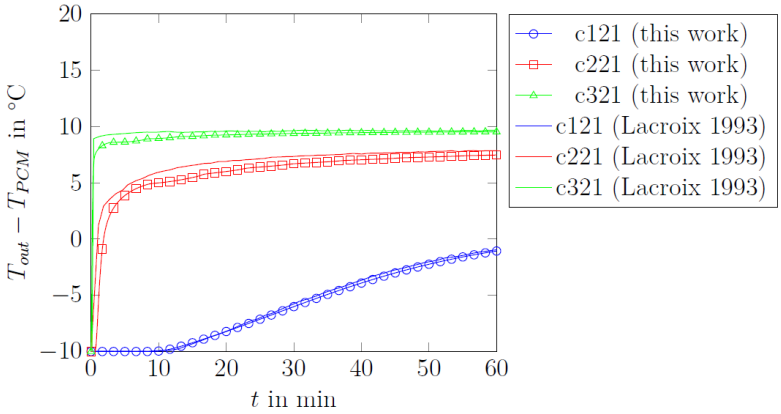

Figure 3.14: Comparison of simulated HTF outlet temperature with $\Delta T = 10$K and $dr_{PCM} = 10.4$mm for different mass flow rates (see Tab. 3.3).

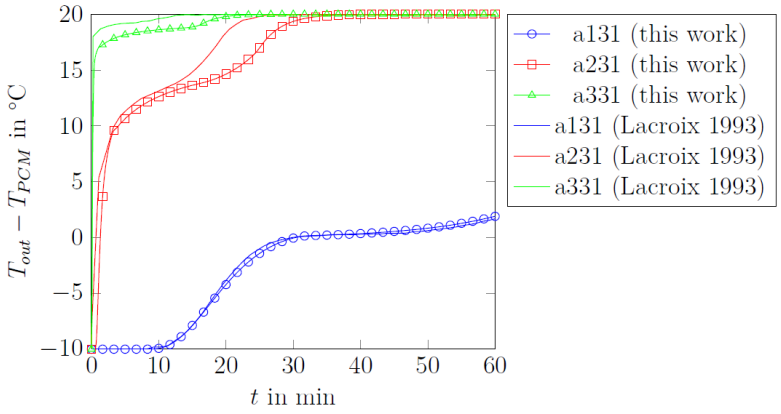

Figure 3.15: Comparison of simulated HTF outlet temperature with $\Delta T = 20$K and $dr_{PCM} = 3.1$mm for different mass flow rates (see Tab. 3.3).

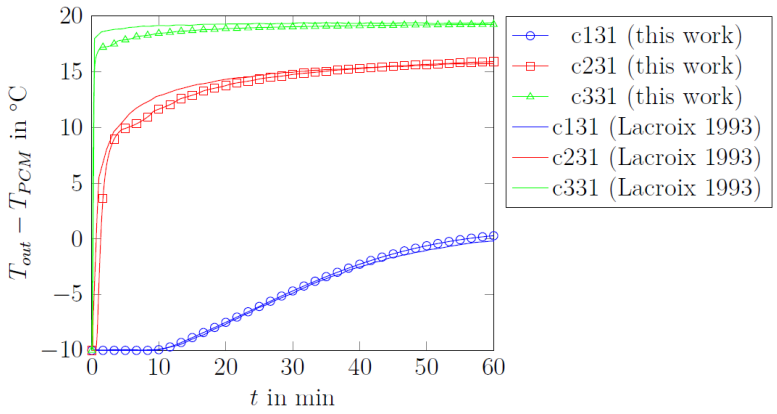

Figure 3.16: Comparison of simulated HTF outlet temperature with $\Delta T = 20\text{K}$ and $dr_{PCM} = 10.4\text{mm}$ for different mass flow rates (see Tab. 3.3).

3.3 Further discussion of simplifications

As was shown previously, it is not clear if all of the simplifications are appropriate. However, it is possible to estimate possible consequences from existing literature (see Table 3.4).

It is interesting to note that the assumption of only conduction heat transfer during melting can be seen as a conservative estimation of the heat transfer rates. For a cold storage, if natural convection is in reality present during melting, the model would underestimate the TES power output during discharging. For a heat storage, the discharge case is solidifying the PCM, which is known as conduction dominated. Moreover, most modeling approaches for PCMs can be seen as macro scale models, since the phase change is not explicitly modeled in micro scale using kinetic laws such as in metal casting [51, 52]. If a micro scale approach is attempted, the model likely depends on the specific type of material (e.g. salt hydrates or paraffins) used as PCM. Research in such detail for these materials would be novel.

Table 3.4: Summary of the major model simplifications and possible consequences on the reliability of the results.

Model Property	Benefit	Possible Consequences
Conduction only	Simple, fast	Under-prediction of heat transfer for melting [20, 53]: • Heat storage: charging • Cold storage: discharging
Phase change using Source Term Method	Near isothermal heat transfer can be treated	PCM proxy model for the Source Term Method is not accurate enough due to limitations of the material characterization method. Phase change is modeled only on a macro scale, while material specific micro scale processes are neglected [51, 52]. No supercooling: Wrong estimation of behavior for recalescence for solidification.[30, 54] • Heat storage: discharging • Cold storage: charging
No momentum balance solved	Simple, fast	Calculation with wrong velocity profile. • Wrong heat transfer estimation from HTF to WALL. • Wrong pressure drop calculation (if included).
TES consists of N identical channels	Simple, fast	Wrong heat transfer estimation due to: • Uneven flow distribution across all channels [55]. • Bulk of PCM movement (during melting) in shell and tube configuration is neglected. • Real design may deviate from a straight plate or tube: e.g. areas of pipe bends or intermediate volumes of PCM between cylindrical shells are not modeled.

Chapter 4

PCM TES Application case

4.1 Definition of Process Conditions

This section shows how the previous model can be used for evaluating different PCM TES designs for an air handling unit (AHU) process (see Fig. 4.1). In the original process, the AHU of an office building is supplied with cold energy from the cooling plant to cover the building cooling demand. Integrating a TES in the system however, would allow a reduction of the amount of cold energy supplied from the cooling plant by charging the TES during the night and supplying cold energy to the AHU via the TES during the day. Potential benefits of using a TES would then be present if the cooling plant can be sized smaller than the actual peak AHU demand and if the price for cold energy production is lower during off-peak hours.

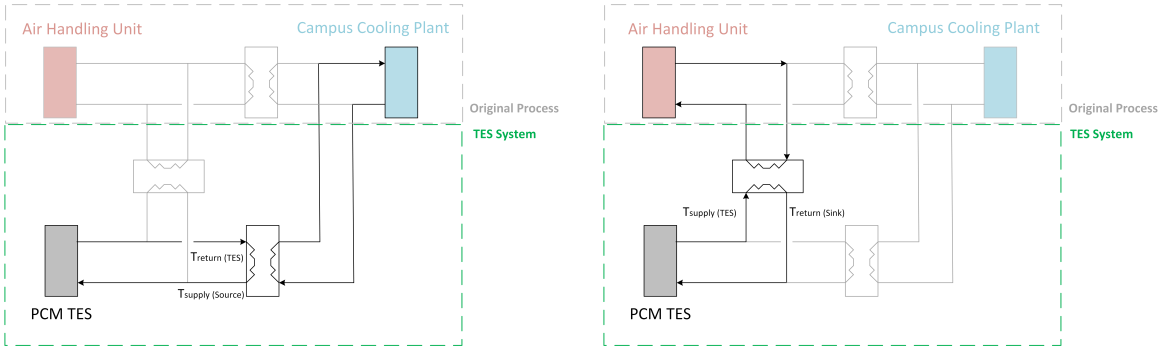

(a) TES charging (b) TES discharging

Figure 4.1: TES integration for a AHU cooling process.

Table 4.1 shows the available temperature of the process source and sink for charging and discharging the storage. The temperature drop of any heat exchangers and piping between the TES and process source/sink are already estimated so that these temperatures correspond to the temperature directly at the storage inlet during charging or discharging. Moreover, it is assumed that these temperatures can be kept constant by e.g. mass flow control downstream of the heat exchangers separating the

Table 4.1: Temperatures for the AHU process

	Value	Comment
T_{supply}^{Source}	8 °C	Constant temperature supplied by the cooling system to the TES inlet during charging.
T_{return}^{Sink}	16 °C	Constant return temperature of the AHU at the TES inlet during discharging.
T_{cutoff}	10 °C	Maximum acceptable temperature by the AHU at the TES outlet during discharging.

TES from the original process. The TES is considered as fully charged at $T = T_{supply}^{Source}$ and fully discharged at $T = T_{return}^{Sink}$. The maximum temperature difference for the TES is then $\Delta T_{max} = 8°C$.

Moreover, the cold energy at the TES outlet during discharging has to be $T_{supply}^{TES} < T_{cutoff}$ in order to be utilizable by the AHU.

If the latent heat of a PCM is to be used as storage material, the latter then has to have a melting temperature within the narrow temperature interval of $T_{supply}^{Source} < T_{PCM} < T_{cutoff}$ in order to be feasible for the process.

For a specified known mass flow rate $\dot{m}$, the achievable power output of the TES is directly given by the HTF temperature difference between inlet and outlet:

$$P_{charging}^{TES}(t) = \dot{m}\ c_p^{HTF}\left|T_{supply}^{Source} - T_{out}(t)\right| \tag{4.1a}$$

$$P_{discharging}^{TES}(t) = \dot{m}\ c_p^{HTF}\left|T_{return}^{Sink} - T_{out}(t)\right| \tag{4.1b}$$

The (dis)charged capacity of the TES over time is then:

$$Q^{TES}(t) = \int_0^t P^{TES}(t)\mathrm{d}t \tag{4.2}$$

$T_{out}(t)$ can be obtained from the model for different cases as demonstrated in the comparison study with the literature model. The design task is then to find the relationships between utilizable power and capacity depending on the TES channel geometry and mass flow rates.

4.2 Definition of PCM TES design parameters

In order to compare different design options it is useful to formulate additional parameters with respect to the process requirements and for the respective scales (see Fig. 4.2). These can be seen as defining the operation characteristics of the TES. The parameters are based on existing work in the literature but slight changes are suggested in the following.

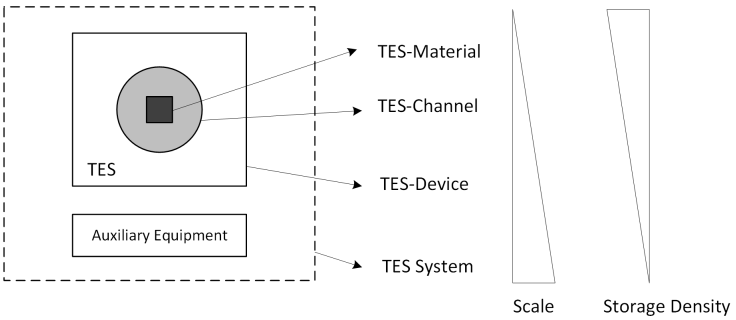

Figure 4.2: Illustration of different scales from the storage material to the TES system. The classification: "material", "device" and "system" originate from ongoing discussions within the IEA ECES Annex 30.

4.2.1 Maximum PCM TES storage density & capacity

A maximum possible storage density δ^i_{max} ($\mathrm{kW\,h\,m^{-3}}$) can be formulated for the individual materials in one channel: $i \in \{HTF, WALL, PCM\}$ using the maximum temperature difference given by the process source and sink (see Fig. 1.3). These materials are considered, since they undergo the same maximum temperature difference when the storage is in its fully charged and discharged state.

$$\delta^i_{max} = \rho^i \cdot c^i_p \cdot \Delta T_{max} + \rho^i \cdot L \tag{4.3}$$

Because HTF and WALL only store sensible heat, the maximum possible channel storage density $\delta^{TES-Channel}_{max}$ is decreased compared to the case where the channel would consist only of PCM ($\delta^{TES-Channel}_{max} < \delta^{PCM}_{max}$).

The reduction in storage density has been defined in previous studies by the terms "porosity" of a TES given by Li et al. 2012 [58] or "compactness" by Amin et al. 2012 [59]. These expressions reflect the reduction in storage density when only the influence of the HTF gap is considered (neglecting the thickness of the WALL).

This idea can be easily extended by using two void factors with respect to the main storage material (in this case PCM), yielding a more general representation for the reduction in storage density. These are given by the channel cross section areas according to Fig. 3.1 and 3.2:

$$\epsilon = \frac{A_{HTF}}{A_{HTF} + A_{PCM} + A_{WALL}} \tag{4.4a}$$

$$\epsilon'' = \frac{A_{WALL}}{A_{PCM} + A_{WALL}} \tag{4.4b}$$

This then leads to the maximum possible storage density for a single channel:

$$\delta_{max}^{TES-Channel} = (1-\epsilon) \cdot \left((1-\epsilon'') \cdot \delta_{max}^{PCM} + \epsilon'' \cdot \delta_{max}^{WALL}\right) + \epsilon \cdot \delta_{max}^{HTF} \tag{4.5}$$

The term $\left((1-\epsilon'') \cdot \delta_{max}^{PCM} + \epsilon'' \cdot \delta_{max}^{WALL}\right)$ expresses the reduction of the maximum possible storage density caused by the heat transfer WALL and the PCM. For a cylindrical geometry, this factor is determined by the thickness of the pipe with respect to the PCM layer thickness. This factor is also a direct measure of the storage density when the PCM is encapsulated.

The void factor ϵ'' can also be used if the PCM domain contains e.g. fins made from WALL material for increased heat transfer. Then the design would be a direct tradeoff between a decreased $\delta_{max}^{TES-Channel}$ against a possible increased power output.

If no other information is available, a first (optimistic) estimate for the storage density of the full scale TES device would be to assume that the TES consists of identical channels:

$$\delta_{max}^{TES} = \delta_{max}^{TES-Channel} \tag{4.6}$$

The maximum possible storage capacity of the TES device is then dependent on the number of channels:

$$V^{TES} = N_{channel} \cdot V^{TES-Channel} \tag{4.7}$$

$$Q_{max}^{TES} = \delta_{max}^{TES} \cdot V^{TES} \tag{4.8}$$

The same can be assumed for the power:

$$P^{TES}(t) = N_{channel} \cdot P^{TES-Channel}(t) = N_{channel} \cdot \dot{m}_{channel} \cdot c_p^{HTF} \cdot (T_{in} - T_{out}(t)) \tag{4.9}$$

All auxiliary equipment, which is necessary for the TES to be operational in the process (such as necessary piping, heat exchangers and pumps connected to the TES), can be included to define the TES System (see system boundary drawn in Fig. 4.1).

When the volume for these are known, the storage density can be even more conservatively estimated:

$$\delta_{max}^{TES-System} = \frac{Q_{max}^{TES}}{V^{TES} + V^{aux}} \tag{4.10}$$

With the definition of an additional system void factor:

$$\epsilon^{TES-System} = \frac{V^{aux}}{V^{TES} + V^{aux}} \tag{4.11}$$

$$\delta_{max}^{TES-System} = (1 - \epsilon^{TES-System}) \cdot \delta_{max}^{TES} \tag{4.12}$$

4.2.2 Effective PCM TES storage density & capacity

In the literature, it is commonly proposed to evaluate and compare thermal energy storages with effectiveness definitions originating from heat exchanger design.

Previous work by Tay et al. and Amin et al. 2012 [59–61] argued that the design of a PCM TES should be evaluated using a "minimum effectiveness" during discharging. The latter represents the "goodness" of heat transfer between the PCM and HTF given by the HTF in- and outlet temperature of the TES. For discharging a PCM cold storage the definition is:

$$\eta_1(t) = \frac{T_{out}(t) - T_{in}}{T_{PCM} - T_{in}} \tag{4.13}$$

The efficiency would then be $\eta_1(t) = 1$ if $T_{out}(t) = T_{PCM}$. Using this definition however, the efficiency may also be $\eta_1 > 1$ if the TES is fully charged below T_{PCM}. A rigorous comparison may be also difficult if the efficiency varies over time. Moreover, a comparison with other storage technologies is not straightforward.

Li et al. 2012 [58], formulated a similarity analysis by studying different idealized TES in terms of a so called "energy delivery effectiveness":

$$\eta_2 = \frac{\int_0^{t_{ref,discharge}} \left| T_{out}(t) - T_{fully,charged} \right| \mathrm{d}t}{\Delta T_{max} \cdot t_{ref,discharge}} \tag{4.14}$$

In their work $t_{ref,discharge}$ is termed as "time period of operation dictated by the needs of the downstream process" and may refer ambiguously to both the required operation period (indirectly meaning the required discharged capacity) as well as the temperature requirements of the process.

Both $\eta_1(t)$ and η_2 quantify the temperature degradation during discharging. η_2 however has the benefit of being constant, as well as including downstream process requirements. A direct evaluation with the previously formulated maximum storage density or capacity is however not straightforward. Moreover, how large the installed storage capacity of a TES should be, is not known beforehand, since the economic optimal size of the TES may be only a fraction of the actual process energy demand.

The efficiency is therefore reformulated with respect to the temperature process requirements only by using T_{cutoff} from the previous chapter as the acceptable temperature limit for T_{out}. Considering the cold storage application, the latter specifies a maximum acceptable temperature by the AHU downstream of the TES. The TES can then only be discharged until the temperature at the TES outlet reaches T_{cutoff}. The cutoff time t' is defined for a discharge case when the outlet temperature reaches the cutoff condition: $T_{out}(t = t') = T_{cutoff}$.

The remaining storage capacity at the point of cutoff can then be considered as redundant and the storage density is further reduced by the factor defined as

capacity efficiency η_Q. It represents the ratio of discharged storage capacity until cutoff ($Q_{eff}^{TES} = \int_0^{t'} P^{TES}(t)\ \mathrm{d}t$) to the maximum possible storage capacity:

$$\eta_Q = \frac{Q_{eff}^{TES}}{Q_{max}^{TES}} \tag{4.15a}$$

$$\delta_{eff}^{TES} = \eta_Q \cdot \delta_{max}^{TES} \tag{4.15b}$$

η_Q is then a factor that can be taken into account both from a technical and economic perspective. If a certain storage capacity Q^{TES} is the design target, the actual storage has to be oversized by $\frac{1}{\eta_Q} \cdot Q^{TES}$ to account for the redundant amount of PCM. The actual PCM material costs for the storage are then also at least by the factor $\frac{1}{\eta_Q}$ higher.

A benefit of defining the operation characteristics this way, is that a TES can then be seen as a "black box" from the process operator point of view. This allows not only the comparison among different PCM TES designs but also with other TES concepts.

For each (dis)charge occasion, the TES could be operated at different constant mass flow rates m_{HTF}^i until the cutoff condition.

A single TES geometry then yields for each m_{HTF}^i a characteristic power curve, capacity and storage density with respect to the downstream process until cutoff:

- time dependent discharge power curve until cutoff: $P_{eff}^i(t)$.
- discharged capacity until cutoff: Q_{eff}^i.
- effective storage density δ_{eff}^i.

It is also useful to characterize the TES in terms of a capacity specific power output following the suggestion from Pinnau and Breitkopf 2015 [27]. The effective power to capacity ratio is then defined in the following as average power output $\left(\overline{P}_{eff}^{TES} = \frac{1}{t'} \int_0^{t'} P^{TES}(t)\mathrm{d}t\right)$ to the discharged capacity until cutoff:

$$\omega_{eff} = \frac{\overline{P}_{eff}^{TES}}{Q_{eff}^{TES}} \tag{4.16}$$

A high or low ω_{eff} may then correspond to whether the TES is utilized to cover peak or base loads within the process. This is useful for comparison if it is not clear which type of TES is optimal for the given process conditions at the beginning of the design process.

4.3 Comparison example of different PCM TES designs

In the following, four TES channel geometries for the AHU process are compared with respect to the previously defined parameters. Since it is assumed that the TES can be charged overnight but to be discharged only during a few hours in the day in order to cover the peak cooling demand, the TES performance is studied based on the discharging case since $P^{TES}_{charging} < P^{TES}_{discharging}$.

Only results for the cylindrical case are presented. The parameters are given in Tab. 4.2 to 4.4 and can be summarized to a TES channel consisting of a HTF pipe (HTF: Water, WALL: Copper) with $5-10$ mm radius with a corresponding $5-10$ mm thick PCM layer. The proxy PCM model is obtained from the commercial RT10HC PCM, which has been measured using T-History experiments in Chapter 2.3, since it melts just between 8 to 10 °C.

It can already be seen that the maximum possible storage density decreases by 10 to 35 % compared to the maximum possible PCM storage density in Tab. 4.4 because a significant volume of the TES channel is filled with water and copper instead of PCM.

Outlet temperature and the corresponding discharge power profiles for a single TES channel are summarized in Fig. 4.3 to 4.6 for all cases. The results are obtained using a mesh of 17200 nodes and a time step of 1 s.

The cutoff time can be read from the figures at the intersection for each $T_{out}(t)$ curve with T_{cutoff}. This is also the relevant duration for the corresponding power curve since the discharged power after the cutoff condition has been reached is not anymore utilizable by the AHU. During the simulated duration of 12 hours, only case *bb11* does not reach this condition because this case exhibits both the lowest flow velocity (largest HTF pipe and lowest mass flow rate) and the largest amount of PCM present.

Table 4.2: TES material parameters. PCM material parameters correspond to the proxy model F1 for RT10HC shown in Fig.2.10.

	This work	Unit	Comment
T_{PCM}	9.6	°C	
T_S	9.35	°C	
T_L	9.85	°C	
L	145	$\mathrm{kJ\,kg^{-1}}$	
λ_S^{PCM}	0.2	$\mathrm{W\,m^{-1}\,K^{-1}}$	
λ_L^{PCM}	0.2	$\mathrm{W\,m^{-1}\,K^{-1}}$	
$c_p^{PCM,solid}$	4600	$\mathrm{J\,kg^{-1}\,K^{-1}}$	
$c_p^{PCM,liquid}$	2600	$\mathrm{J\,kg^{-1}\,K^{-1}}$	
ρ^{PCM}	770	$\mathrm{kg\,m^{-3}}$	
λ^{WALL}	300	$\mathrm{W\,m^{-1}\,K^{-1}}$	estimated for copper [57]
c_p^{WALL}	385	$\mathrm{J\,kg^{-1}\,K^{-1}}$	estimated for copper [57]
ρ^{WALL}	8900	$\mathrm{kg\,m^{-3}}$	estimated for copper [57]
λ^{HTF}	0.6	$\mathrm{W\,m^{-1}\,K^{-1}}$	estimated for water [50]
c_p^{HTF}	4180	$\mathrm{J\,kg^{-1}\,K^{-1}}$	estimated for water [50]
ρ^{HTF}	1000	$\mathrm{kg\,m^{-3}}$	estimated for water [50]

Table 4.3: Simulated cases for the AHU process. The radial thickness dr_i corresponds to Fig. 3.1.

r_{HTF} in mm	Tag 1	dr_{PCM} in mm	Tag 2	$\dot{m}$ in $\mathrm{kg\,s^{-1}}$	Tag 3	t_{end} in h	Tag 4
5	a	5	a	0.7×10^{-4}	1	12	1
10	b	10	b	1.0×10^{-4}	2		
				1.3×10^{-4}	3		

Table 4.4: Constant simulation parameters for all cases. The radial thickness dr_i corresponds to Fig. 3.1.

Case independent parameters	Value	Unit	Comment
T^0	8	°C	
T_{in}	16	°C	
Axial length	1	m	
dr_{WALL}	1	mm	
h_{WALL}	219.6	$\mathrm{W\,m^{-2}\,K^{-1}}$	for cases $aXXX$
	109.8	$\mathrm{W\,m^{-2}\,K^{-1}}$	for cases $bXXX$
δ_{max}^{PCM}	36.1	$\mathrm{kW\,h\,m^{-3}}$	for PCM proxy model F1
δ_{max}^{TES}	28.0	$\mathrm{kW\,h\,m^{-3}}$	for cases $aaXX$
	32.3	$\mathrm{kW\,h\,m^{-3}}$	for cases $abXX$
	23.3	$\mathrm{kW\,h\,m^{-3}}$	for cases $baXX$
	28.7	$\mathrm{kW\,h\,m^{-3}}$	for cases $bbXX$

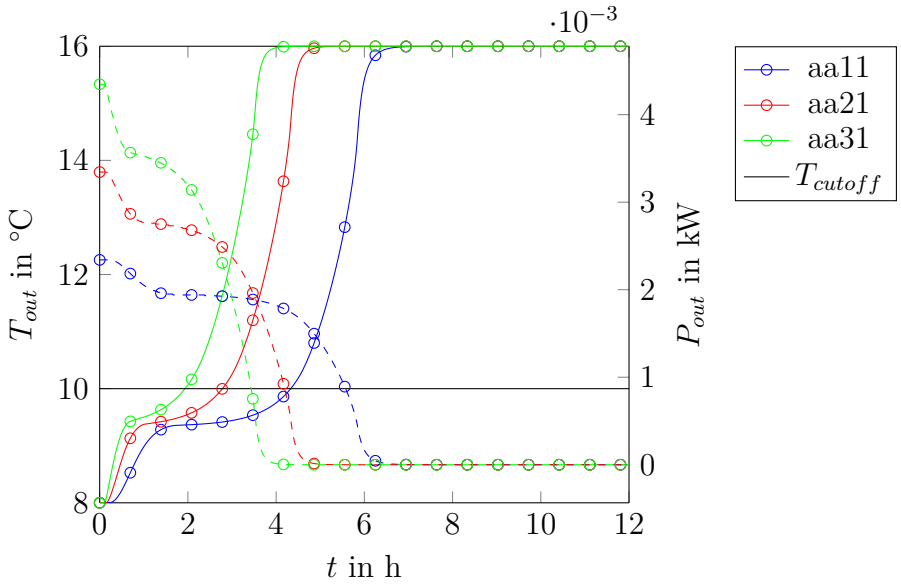

Figure 4.3: Simulated HTF outlet temperatures and power for different mass flow rates (Cases $aaXX$ (from Tab. 4.3), solid lines: T_{out}, dashed lines: P_{out}).

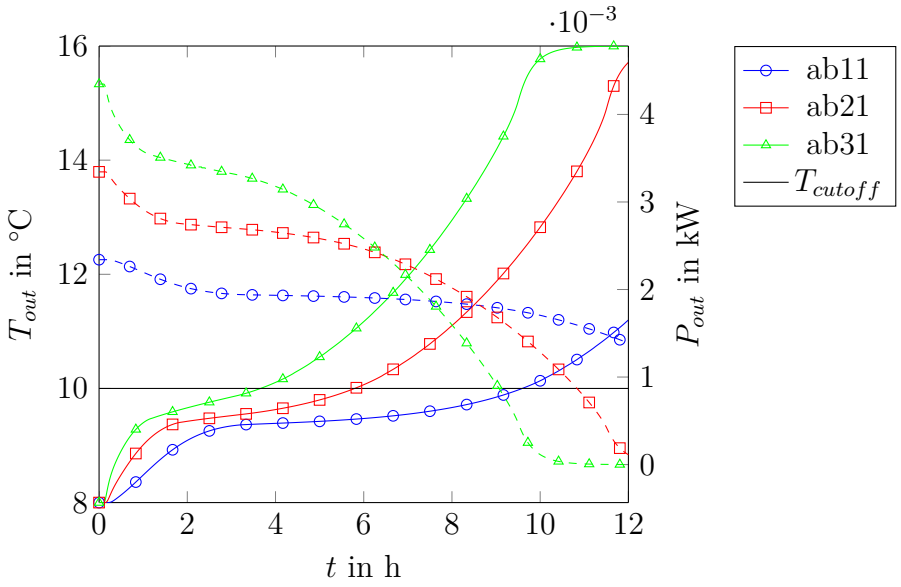

Figure 4.4: Simulated HTF outlet temperatures and power for different mass flow rates (Cases *abXX* (from Tab. 4.3), solid lines: T_{out}, dashed lines: P_{out}).

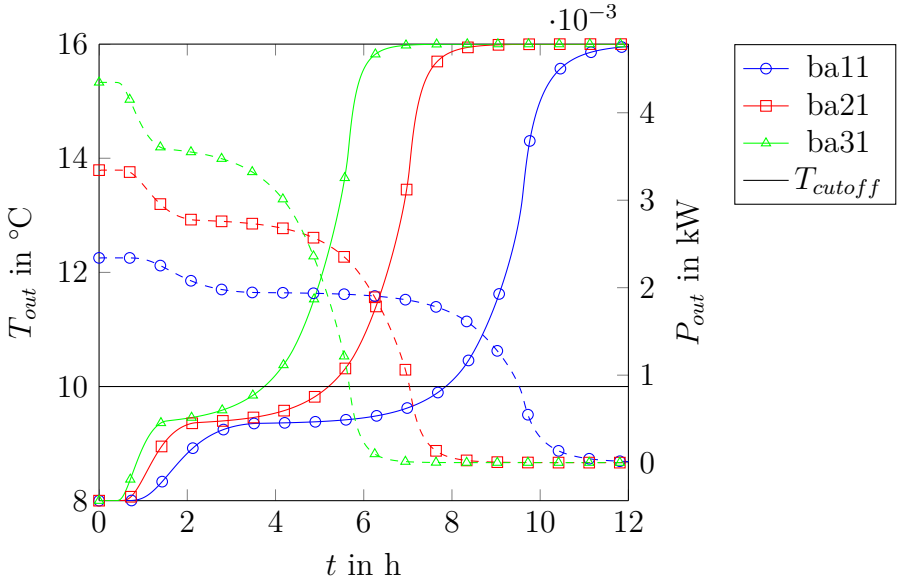

Figure 4.5: Simulated HTF outlet temperatures and power for different mass flow rates (Cases *baXX* (from Tab. 4.3), solid lines: T_{out}, dashed lines: P_{out}).

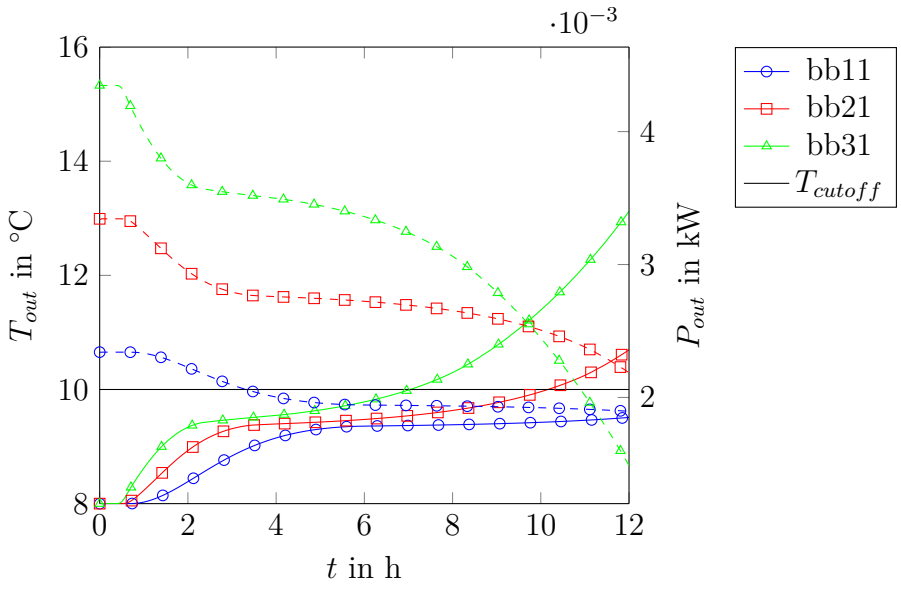

Figure 4.6: Simulated HTF outlet temperatures and power for different mass flow rates (Cases *bbXX* (from Tab. 4.3), solid lines: T_{out}, dashed lines: P_{out}).

Tab. 4.5 and 4.6 summarize the different geometries operated at the three mass flow rates based on the previously formulated parameters in terms of the cutoff condition (see Chapter 4.2). From the results, a few important conclusions can be drawn.

Table 4.5: Summary of PCM TES design parameters for cases *aXXX*.

	aa11	aa21	aa31	ab11	ab21	ab31	Unit
t_{eff}	4.33	2.78	1.93	9.59	5.79	3.66	h
η_Q	0.81	0.73	0.66	0.72	0.62	0.50	-
$\overline{P}_{eff}^{TES}$	2.0	2.8	3.6	2.0	2.8	3.5	W (per channel)
Q_{eff}^{TES}	8.6	7.8	7.0	18.8	16	13.0	W h (per channel)
δ_{max}^{TES}	28	28	28	32.3	32.3	32.3	$\mathrm{kW\,h\,m^{-3}}$
δ_{eff}^{TES}	22.7	20.6	18.4	23.4	19.9	16.1	$\mathrm{kW\,h\,m^{-3}}$
ω_{eff}	231	360	517	104	173	273	$\mathrm{W\,kW^{-1}\,h^{-1}}$

Table 4.6: Summary of PCM TES design parameters for cases *bXXX*.

	ba11	ba21	ba31	bb11	bb21	bb31	Unit
t_{eff}	7.86	5.20	3.74	-	10.16	7.04	h
η_Q	0.84	0.79	0.74	-	0.72	0.64	-
$\overline{P}_{eff}^{TES}$	2.0	2.9	3.7	-	2.8	3.6	W (per channel)
Q_{eff}^{TES}	15.8	14.9	13.8	-	28.5	25.4	W h (per channel)
δ_{max}^{TES}	23.3	23.3	23.3	28.7	28.7	28.7	$\mathrm{kW\,h\,m^{-3}}$
δ_{eff}^{TES}	19.7	18.5	17.2	-	20.6	18.3	$\mathrm{kW\,h\,m^{-3}}$
ω_{eff}	127	192	267	-	98	142	$\mathrm{W\,kW^{-1}\,h^{-1}}$

- From Tab. 4.5 and 4.6 it can be seen that within each geometry, increasing the mass flow rate yields a higher average power output. There is however a trade-off with a lower capacity efficiency since the time of cutoff is reached sooner at higher mass flow rates. Therefore, even doubling the PCM layer does not necessarily increase the effective storage density, if the TES is operated at a too high mass flow rate (e.g. compare cases *aa21* with *ab21* or *aa31* with *ab31*).

  In order to obtain the same range of capacity effectiveness, the mass flow rate has to be decreased when the PCM layer is increased from 0.5 to 1 cm (e.g.

compare case *aa21* with *ab11* as well as case *ba31* with *bb21*). This is also reflected by a smaller effective power to capacity number ω_{eff}.

- It is moreover interesting to note that the higher flow velocity for the cases with the smaller HTF pipe diameter (cases *aXXX*) does not affect the efficiency compared to lower flow velocities of the larger HTF pipe (cases *bXXX*) for the same mass flow rates. This can be explained by the used constant Nusselt number correlation yielding a factor two increase of the wall heat transfer coefficient (see Tab. 4.4). Because the thermal resistance of the copper pipe is very small, the thermal resistance across the WALL domain is essentially determined by h_{WALL}. Increasing the heat transfer coefficient between HTF and PCM was therefore beneficial for both increasing the power output and effective storage density.

  Since the single channel power profiles for all cases are only in the range of $1 - 5$ W, a significant number of identical channels are needed to reach power outputs in the range of kilowatts.

- Fig. 4.7 shows the PCM domain at $t = t_{cutoff}$ for the cases *ab11* and *ab31*, which yielded large differences in η_Q. It can be seen that the capacity efficiency directly corresponds to the shape of the melting front. Case *ab11*, which has the higher efficiency, is much closer to a so called 1-D melting front [62] compared to case *ab31*. This means in order for the PCM TES to be efficient, the TES should be designed and operated such that the phase change propagates with a more vertical front with respect to the axial length of the channel.

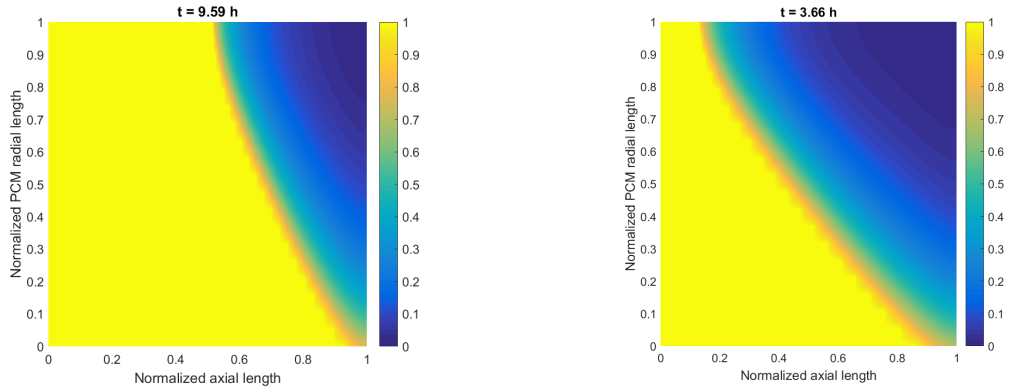

(a) Case *ab11*: $\eta_Q = 0.72$ (b) Case *ab31*: $\eta_Q = 0.5$

Figure 4.7: Liquid fraction in the PCM domain at t_{cutoff} for two simulated cases.

This is convenient from a design perspective, since the storage capacity can then be increased approximately linearly with the channel axial length (which has been abritarily fixed to 1 m in this study), while keeping the power and capacity efficiency constant. This leads to other possible values for w_{eff} without changing the channel radial geometries.

However, it is likely that this requirement can be relaxed more towards two dimensional melting if the cutoff temperature is set higher with respect to the PCM melting temperature.

4.3.1 Comparison with a perfectly mixed water tank TES model

In order to exemplify that the performance characteristics can be evaluated for any type of TES, the process parameters are briefly studied using a simple lumped model applied to the AHU process:

$$ {c_p}^{water} m_{water} \frac{dT_{TES}}{dt} = \dot{m}_{HTF}\ {c_p}^{HTF} \left(T_{in} - T_{TES}(t)\right) \tag{4.17} $$

Eq. 4.17 can be seen as a model for discharging a water tank, where at the inlet, water at $T_{in} = 16°C$ is supplied at a constant mass flow rate. The tank is then assumed to be of uniform temperature ($ {c_p}^{water} = {c_p}^{HTF} = 4180 \mathrm{J\,kg^{-1}\,K^{-1}} $ and perfectly mixed). The outlet temperature is then $T_{out}(t) = T_{TES}(t)$ and severe temperature degradation inside the TES occurs due to mixing with the inlet water from $T_{TES}(t = 0) = T^0 = 8°C$ (its fully charged state) to $T_{TES} = T_{in} = 16°C$, when the storage is fully discharged.

For the previously studied cases *aaXX*, the maximum possible storage capacity of a single channel is $Q_{max}^{TES-channel} = 10.6 \mathrm{W\,h}$ stemming from the PCM, WALL and HTF material and the maximum temperature difference $\Delta T_{max} = 8K$. To achieve the same maximum storage capacity for the lumped model, the mass of water as storage material has to be $m_{water} = \frac{Q_{max}^{TES-channel}}{{c_p}^{water} \Delta T_{max}} = 1.14 kg$.

Eq. 4.17 can be solved easily for the same constant mass flow rates as in Tab. 4.3. And the results are summarized in Fig. 4.8 and Tab. 4.7.

Table 4.7: Summary of lumped water tank TES design parameters for three different mass flow rates: *1, 2, 3* (Tag 3) of Tab. 4.3.

	1	*2*	*3*	Unit
t_{eff}	1.30	0.91	0.70	h
η_Q	0.25	0.25	0.25	
$\overline{P}_{eff}^{TES}$	2.0	2.9	3.8	W
Q_{eff}^{TES}	2.65	2.65	2.65	W h
δ_{max}^{TES}	9.29	9.29	9.29	$\mathrm{kW\,h\,m^{-3}}$
δ_{eff}^{TES}	2.32	2.32	2.32	$\mathrm{kW\,h\,m^{-3}}$
ω_{eff}	768	1097	1426	$\mathrm{W\,kW^{-1}\,h^{-1}}$

A low capacity efficiency of 0.25 is obtained for all mass flow rates but with a trade-off between a high average discharge power or longer cutoff time. The low

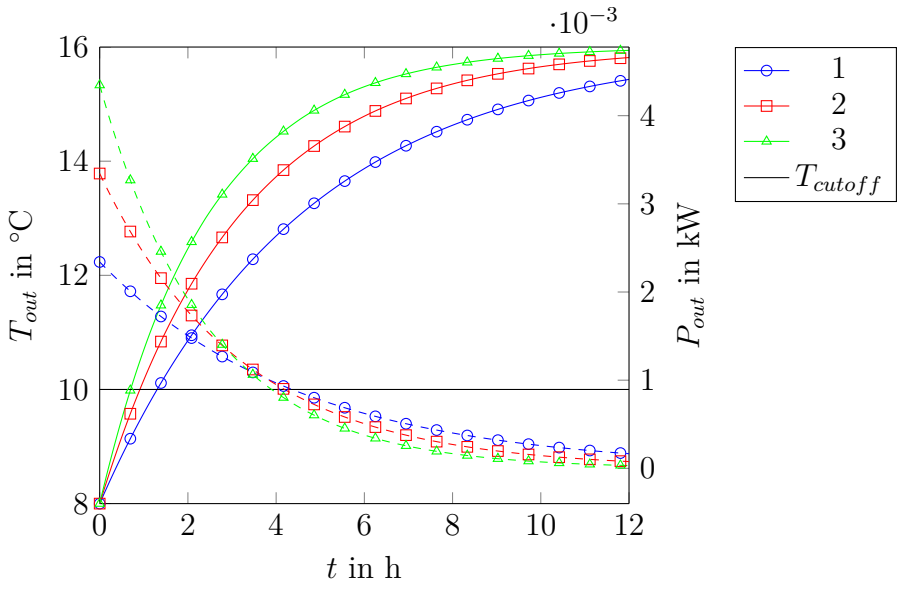

Figure 4.8: Simulated HTF outlet temperatures and power for the lumped TES model for three different mass flow rates: *1, 2, 3* (Tag 3) of Tab. 4.3. (Solid lines: T_{out}, dashed lines: P_{out}).

efficiency is a direct consequence of the perfect mixing assumption and causes a worse performance compared to the previous PCM TES cases. The model can be obviously replaced with much more accurate representations of a water tank (e.g. by including a vertical temperature distribution in the tank [2]) and again compared against the PCM TES design.

4.4 Effect of input uncertainties on the TES model results

In the following, the effect of uncertainties in the input parameters are studied based on case *aa21* from the previous study. An analysis of the latter is useful in order to predict the model sensitivity of important design parameters such as the capacity efficiency for variations of the model input parameters.

In the first case, the heat transfer coefficient h_{WALL} is assumed to be either $\approx 50\%$ less than the calculated one from $Nu = 3.66$ or to be very large, representing an negligible heat transfer resistance between HTF and WALL.

In another case, a conservative proxy PCM model is used to account for material uncertainties:

- The real phase change temperature could be closer to T_{cutoff} leaving a smaller temperature difference for heat transfer. Then T_{PCM} should be fitted closer to the heating curve from the hysteresis (see e.g. Proxy model F3 in Fig. 2.10).

- The sensible heat capacity and latent heat could be in reality smaller than measured by the T-History method.

The latent heat can be conservatively estimated by performing the same Monte Carlo simulations as in **Paper 2**. From Fig. 4.9 it is assumed that the variations of the enthalpy value across the phase change temperature is normal distributed. An expanded uncertainty can then be given using a $k = 2$ coverage factor (95 % confidence interval): $h_{12-7°C} = -165.5\ \mathrm{kJ\,kg^{-1}}$ $(1 \pm 5.3\%)$. The relative expanded uncertainty is then used to estimate the latent heat of the proxy model: $L = 145\ \mathrm{kJ\,kg^{-1}}$ $(1 \pm 5.3\%)$. A conservative estimate is then: $L = 137.32\ \mathrm{kJ\,kg^{-1}}$.

Moreover, it is unclear which specific heat capacity in the sensible and liquid phase for RT10HC should be used since both T-History and the official data sheet give contradicting values [63]. The T-History results of $c_p^S = 4600\mathrm{J\,kg^{-1}\,K^{-1}}$ and $c_p^L = 2600\mathrm{J\,kg^{-1}\,K^{-1}}$ are likely overestimations as outlined in **Paper 1**. Therefore the lowest available data sheet value of $c_p = 2000\mathrm{J\,kg^{-1}\,K^{-1}}$ is used for both liquid and solid phase [63].

The parameter variations are summarized in Tab. 4.8.

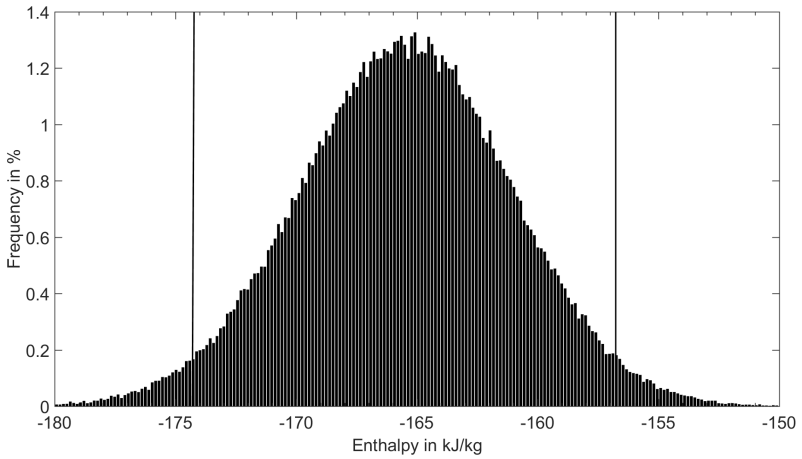

Figure 4.9: Estimated uncertainty for $\Delta h_{12-7°C}$ of RT10HC using a 95 % coverage interval from the frequency distribution of $N = 200,000$ Monte Carlo trials from **Paper 2**. $h_{12-7°C} = -165.5 \pm 8.7\mathrm{kJ\,kg^{-1}}$ (expanded uncertainty $k = 2$).

Table 4.8: Summary of input parameter variations for the case *aa21* compared to Ch. 4.3.

Parameter	hWall100	hWall10000	PCMconsersative	
h_{WALL}	100	1e4	unchanged	$\mathrm{W\,m^{-2}\,K^{-1}}$
T_{PCM}	unchanged	unchanged	9.75	°C
L	unchanged	unchanged	137.32	$\mathrm{kJ\,kg^{-1}}$
c_p^S,c_p^L	unchanged	unchanged	2000	$\mathrm{J\,kg^{-1}\,K^{-1}}$

Fig. 4.10 and Tab. 4.9 summarize the simulation results for the different cases. Decreasing the heat transfer coefficient as well as the conservative PCM proxy model

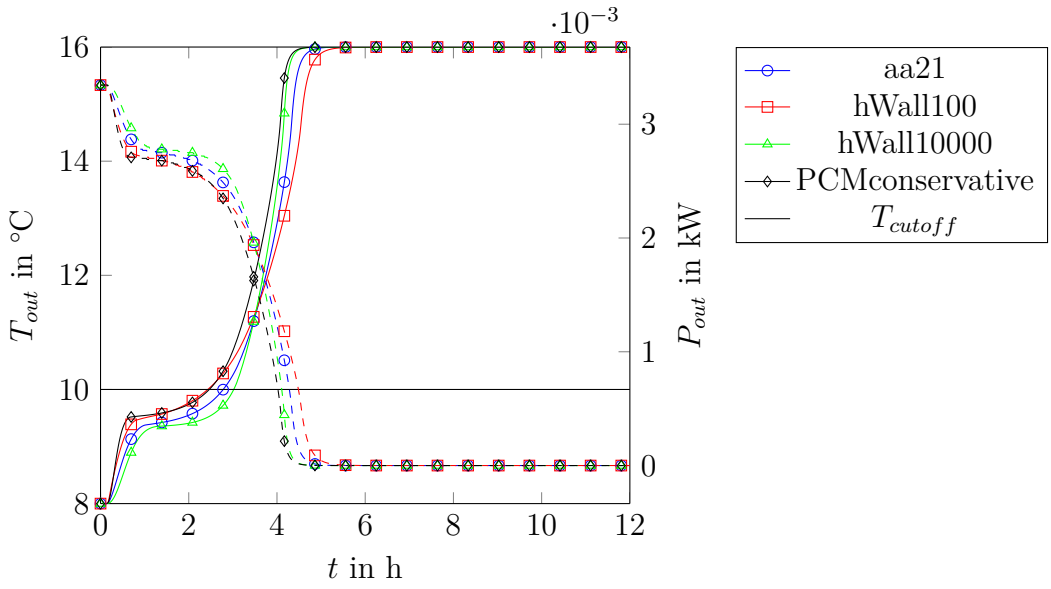

Figure 4.10: Simulated HTF outlet temperatures and power for different mass flow rates (solid lines: T_{out}, dashed lines: P_{out}).

Table 4.9: Summary of input parameter variations of case *aa21*.

	aa21	hWall100	hWall10000	PCMconsersative	Unit
t_{eff}	2.78	2.43	3.02	2.47	h
η_Q	0.73	0.63	0.81	0.70	-
δ_{max}^{PCM}	36.1	36.1	36.1	32.7	$\mathrm{kW\,h\,m^{-3}}$
δ_{max}^{TES}	28.0	28.0	28.0	25.6	$\mathrm{kW\,h\,m^{-3}}$
δ_{eff}^{TES}	20.6	17.7	22.6	17.8	$\mathrm{kW\,h\,m^{-3}}$
ω_{eff}	360	411	331	406	$\mathrm{W\,kW^{-1}\,h^{-1}}$

yield both a decrease of the capacity efficiency. Interesting is that the results are more sensitive to a decrease of h_{WALL} than assuming a negligible heat transfer resistance at the wall. This is because the heat transfer is overall limited due to the low thermal conductivity of the PCM even if a near perfect heat transfer at the HTF and WALL boundary is assumed.

Therefore, a realistic representation of the heat transfer within the PCM domain itself, such as a realistic value of the PCM thermal conductivity or the inclusion of natural convection of the liquid phase during melting are important for accurate results.

Decreasing the solid specific heat capacity from 4600 to 2000 $\mathrm{J\,kg^{-1}\,K^{-1}}$ does not have a significant effect since the temperature difference between T^0 and T_{cutoff} is only 2K. The decrease of the capacity efficiency for the conservative proxy model is likely due to the higher melting temperature and smaller temperature difference to the cutoff condition.

4.5 Conclusions & Outlook for the PCM TES device design

In the end, a feasible geometry and operational mass flow rate have to be determined based on the costs of the PCM TES consisting of at least the material costs, e.g. for the PCM and copper pipes. All relevant cost factors in choosing a PCM TES design have to be then weighted against the potential process specific benefits when operating the storage. The latter are given e.g. by the net benefit for each discharge occasion depending on the on- and off-peak energy prices as well as the varying cold demand of the AHU in the office building over a year. It is then crucial that the costs for charging the storage (which may also depend on the outlet temperature) have to be analyzed as well. This should also include an estimate of the pressure drops in the storage.

The current model assumes adiabatic conditions. However, if the duration between charging and discharging the TES is long, heat losses have to be included depending on the existing level of the insulation. Then the cost for applying different magnitudes of insulation around the TES have to be traded off against costs associated with the heat losses to the ambient. For estimating these (and the above mentioned pressure drops), however, the size of the TES has to be determined first. Heat losses will also lead to different operational characteristics, since then the initial temperature at the start of a discharge occasion is higher compared to the charging temperature. The results presented in this chapter can be seen as necessary input data for the future work on system level that translates each potential case into economic and ecological parameters. For a higher reliability of the data, the simulated performance curves should be replaced by experimental data using prototypes or full scale TES whenever available.

Although rectangular cases are not presented, the same conclusions as above can also be drawn for the latter geometry. Depending on how the two geometries differ in purchase costs and performance, a rigorous comparison between the two geometrical options may be necessary.

Chapter 5

Final Conclusions & Future work

Based on the studied integration case, final conclusions and further recommendations can be made to address the limitations of the framework discussed in Chapter 1.

Material level

The PCM was chosen for the AHU case based on the given available temperature levels of the process. Due to the narrow temperature interval, only the paraffin based RT10HC PCM was measured as suitable using the T-History method. As was shown in Chapter 2, the current method allows repeatable results in terms of generating an enthalpy-temperature curve for PCMs. The results however are still subject to systematic errors, since the mathematical model is only a simplification. Until these systematic errors are corrected, it is recommended to evaluate the results using other sources whenever possible. This can be seen as a general recommendation until measurement standards for PCMs are established.

Device level

The material level results are used to develop PCM proxy models for the simulation on device level. For the latter, it is assumed that the TES consists of a number of identical channels in order to make the design methodology scalable. A single channel was then evaluated for the given temperature levels of an AHU application using different mass flow rates of the HTF and performance parameters were formulated based on existing literature.

It is important to note that the formulated parameters based on a cutoff condition in this work can also be used for other types of TES (e.g. sensible heat TES), making a comparison between them possible. It would be also interesting to consider (dis)charging any TES with non-constant mass flow rates in future work to increase the usable storage capacity. The mass flow control should then be based directly on predefined temperature requirements of the HTF at the TES outlet. For example, if the cutoff temperature condition is exceeded during operation, the mass flow rate could be decreased, so that the remaining PCM still can be utilized but at a reduced power.

For the AHU process, only one commercial PCM was considered, since the available temperature difference in the process was narrow. If a wider temperature difference would be available, the selection of the PCM with different melting points increases the design choices further.

The temperature difference could be widened, if it is deemed acceptable to mix the TES outlet flow with an additional thermal energy source downstream of the TES during discharging. The cutoff temperature at the TES outlet itself is then seen as an additional design parameter. The increased costs for this approach then likely have to be weighted against decreased TES design costs resulting from a relaxed cutoff condition.

In order to validate and improve the developed TES model, future work will focus on verifying the observations of the simulation study based on laboratory scale experiments of a PCM TES. It would be useful to clearly separate the uncertainties in material properties from the simplifications done in the heat transfer model, in order to find the range of applicability of the model simplifications. Further work should also focus on a methodology to optimize a single channel geometry for a desired target power output and capacity.

System level

It was concluded that the system level optimization needs to systematically evaluate economic and ecological factors stemming from the different design options. This can be seen as an optimization task to find the approximate TES size (installed capacity & power) and operation schedule, which maximizes the TES net benefits. This will also lead to the economic limits for when a PCM TES integration becomes feasible. A new set of parameters may then be formulated to evaluate the "goodness" of the final process. An example would be calculating the payback period for investing in a TES.

This is an important part of the future work since only then a decision can be made which PCM choice, TES channel geometry, number of channels and mass flow rate is the optimum for the process. Moreover, other relevant parameters for each design choice have to be evaluated. This may include safety (e.g. flammability) and reliability (e.g. PCM leakages) concerns of the storage. It may also be useful to rank these parameters based on their importance for the given process from the perspective of different stakeholders involved in the design process.

Since each level by itself is still an active field of research, the outcome of any design methodology at present can only be as good as the reliability of its current assumptions. Based on the previous discussion around Fig. 1.7 of Chapter 1, the framework can be seen as a continuous work in progress, which should allow the inclusion of more accurate data and feasible design options whenever available.

References

[1] International Energy Agency. *Technology Roadmap: Energy Storage*. 2014 (cit. on p. 3).

[2] Dinçer, İ. and Rosen, M. *Thermal energy storage: Systems and applications*. 2nd ed. Hoboken, N.J.: Wiley, 2011. ISBN: 0470970758 (cit. on pp. 3, 7, 57).

[3] Kousksou, T. et al. "Energy storage: Applications and challenges". In: *Solar Energy Materials and Solar Cells* 120 (2014), pp. 59–80. ISSN: 09270248. DOI: 10.1016/j.solmat.2013.08.015 (cit. on p. 3).

[4] Aneke, M. and Wang, M. "Energy storage technologies and real life applications – A state of the art review". In: *Applied Energy* 179 (2016), pp. 350–377. ISSN: 03062619. DOI: 10.1016/j.apenergy.2016.06.097 (cit. on p. 3).

[5] Arteconi, A. et al. "State of the art of thermal storage for demand-side management". In: *Applied Energy* 93 (2012), pp. 371–389. ISSN: 03062619. DOI: 10.1016/j.apenergy.2011.12.045 (cit. on p. 3).

[6] Mehling, H. and Cabeza, L. F. *Heat and cold storage with PCM: An up to date introduction into basics and applications; with 28 tables*. Heat and Mass Transfer. Springer, 2008. ISBN: 354068557X (cit. on pp. 3, 4, 13–15).

[7] Zalba, B. et al. "Review on thermal energy storage with phase change: materials, heat transfer analysis and applications". In: *Applied Thermal Engineering* 23.3 (2003), pp. 251–283. ISSN: 13594311. DOI: 10.1016/S1359-4311(02)00192-8 (cit. on pp. 3, 4).

[8] Cabeza, L. F. et al. "Materials used as PCM in thermal energy storage in buildings: A review". In: *Renewable and Sustainable Energy Reviews* 15.3 (2011), pp. 1675–1695. ISSN: 13640321. DOI: 10.1016/j.rser.2010.11.018 (cit. on pp. 3, 4).

[9] Hyun, D. C. et al. "Emerging Applications of Phase-Change Materials (PCMs): Teaching an Old Dog New Tricks". In: *Angewandte Chemie International Edition* 53.15 (2014), pp. 3780–3795. ISSN: 1521-3773. DOI: 10.1002/anie.201305201 (cit. on p. 3).

[10] Agyenim, F. B. et al. "A review of materials, heat transfer and phase change problem formulation for latent heat thermal energy storage systems (LHTESS)". In: *Renewable and Sustainable Energy Reviews* 14.2 (2010), pp. 615–628. ISSN: 13640321. DOI: 10.1016/j.rser.2009.10.015 (cit. on p. 4).

[11] Pereira da Cunha, J. and Eames, P. "Thermal energy storage for low and medium temperature applications using phase change materials – A review". In: *Applied Energy* 177 (2016), pp. 227–238. ISSN: 03062619. DOI: 10.1016/j.apenergy.2016.05.097 (cit. on p. 4).

[12] Zhou, D. et al. "Review on thermal energy storage with phase change materials (PCMs) in building applications". In: *Applied Energy* 92 (2012), pp. 593–605. ISSN: 03062619. DOI: 10.1016/j.apenergy.2011.08.025 (cit. on p. 4).

[13] Whiffen, T. R. and Riffat, S. B. "A review of PCM technology for thermal energy storage in the built environment: Part II". In: *International Journal of Low-Carbon Technologies* 8.3 (2013), pp. 159–164. ISSN: 1748-1317. DOI: 10.1093/ijlct/cts026 (cit. on p. 4).

[14] Rathgeber, C. et al. "IEA SHC Task 42 / ECES Annex 29 – A Simple Tool for the Economic Evaluation of Thermal Energy Storages". In: *Energy Procedia* 91 (2016), pp. 197–206. ISSN: 18766102. DOI: 10.1016/j.egypro.2016.06.203 (cit. on p. 5).

[15] Whiffen, T. R. and Riffat, S. B. "A review of PCM technology for thermal energy storage in the built environment: Part I". In: *International Journal of Low-Carbon Technologies* 8.3 (2013), pp. 147–158. ISSN: 1748-1317. DOI: 10.1093/ijlct/cts021 (cit. on p. 5).

[16] Cabeza, L. F. et al. "Unconventional experimental technologies available for phase change materials (PCM) characterization. Part 1. Thermophysical properties". In: *Renewable and Sustainable Energy Reviews* 43 (2015), pp. 1399–1414. ISSN: 13640321. DOI: 10.1016/j.rser.2014.07.191 (cit. on pp. 6, 13).

[17] Inés Fernández, A. et al. "Unconventional experimental technologies used for phase change materials (PCM) characterization: part 2 – morphological and structural characterization, physico-chemical stability and mechanical properties". In: *Renewable and Sustainable Energy Reviews* 43 (2015), pp. 1415–1426. ISSN: 13640321. DOI: 10.1016/j.rser.2014.11.051 (cit. on pp. 6, 14).

[18] Ibrahim, N. I. et al. "Heat transfer enhancement of phase change materials for thermal energy storage applications: A critical review". In: *Renewable and Sustainable Energy Reviews* 74 (2017), pp. 26–50. ISSN: 13640321. DOI: 10.1016/j.rser.2017.01.169 (cit. on p. 6).

[19] Castell, A. and Solé, C. "An overview on design methodologies for liquid–solid PCM storage systems". In: *Renewable and Sustainable Energy Reviews* 52 (2015), pp. 289–307. ISSN: 13640321. DOI: 10.1016/j.rser.2015.07.119 (cit. on pp. 6, 31).

[20] Dutil, Y. et al. "A review on phase-change materials: Mathematical modeling and simulations". In: *Renewable and Sustainable Energy Reviews* 15.1 (2011), pp. 112–130. ISSN: 13640321. DOI: 10.1016/j.rser.2010.06.011 (cit. on pp. 6, 8, 12, 34, 41).

[21] Dinçer, İ. and Rosen, M. *Exergy: Energy, environment and sustainable development / Ibrahim Dincer, Marc A. Rosen*. 2nd ed. Oxford: Elsevier Science, 2013. ISBN: 0080970893 (cit. on p. 7).

[22] *ASHRAE handbook: Heating, ventilating, and air-conditioning applications*. SI ed. Atlanta, Ga.: ASHRAE, 2012. ISBN: 193650426X (cit. on p. 7).

[23] Cole, W. J. et al. "Optimization and advanced control of thermal energy storage systems". In: *Reviews in Chemical Engineering* 28.2-3 (2012). ISSN: 2191-0235. DOI: 10.1515/revce-2011-0018 (cit. on p. 7).

[24] Sun, Y. et al. "Peak load shifting control using different cold thermal energy storage facilities in commercial buildings: A review". In: *Energy Conversion and Management* 71 (2013), pp. 101–114. ISSN: 01968904. DOI: 10.1016/j.enconman.2013.03.026 (cit. on p. 7).

[25] Yu, Z. et al. "Control strategies for integration of thermal energy storage into buildings: State-of-the-art review". In: *Energy and Buildings* 106 (2015), pp. 203–215. ISSN: 03787788. DOI: 10.1016/j.enbuild.2015.05.038 (cit. on p. 7).

[26] Rathgeber, C. et al. "Economic top–down evaluation of the costs of energy storages—A simple economic truth in two equations". In: *Journal of Energy Storage* 2 (2015), pp. 43–46. ISSN: 2352152X. DOI: 10.1016/j.est.2015.06.001 (cit. on p. 7).

[27] Pinnau, S. and Breitkopf, C. "Determination of Thermal Energy Storage (TES) characteristics by Fourier analysis of heat load profiles". In: *Energy Conversion and Management* 101 (2015), pp. 343–351. ISSN: 01968904. DOI: 10.1016/j.enconman.2015.05.055 (cit. on pp. 7, 48).

[28] International Energy Agency. *Energy Conservation through Energy Storage (ECES): Annex 30 (Thermal Energy Storage for Cost-Effective Management and CO2 Mitigation): Work Program*. 2016. URL: http://www.eces-a30.org/ (cit. on p. 7).

[29] Günther, E. et al. "Determination of the heat storage capacity of PCM and PCM-objects as a function of temperature". In: *Proceedings of ECOSTOCK, 10th International Conference on Thermal Energy Storage*. 2006 (cit. on p. 14).

[30] Rathgeber, C. et al. "Analysis of supercooling of phase change materials with increased sample size – Comparison of measurements via DSC, T-History and at pilot plant scale". In: *Greenstock 2015 - 13th IEA ECES Conference* (cit. on pp. 14, 41).

[31] Rathgeber, C. et al. "Measurement of enthalpy curves of phase change materials via DSC and T-History: When are both methods needed to estimate the behaviour of the bulk material in applications?" In: *Thermochimica Acta* 596 (2014), pp. 79–88. ISSN: 0040-6031. DOI: 10.1016/j.tca.2014.09.022 (cit. on pp. 14, 15).

[32] Günther, E. et al. “Modeling of subcooling and solidification of phase change materials”. In: *Modelling and Simulation in Materials Science and Engineering* 15.8 (2007), pp. 879–892. ISSN: 0965-0393. DOI: 10.1088/0965-0393/15/8/005 (cit. on p. 14).

[33] Stefanescu, D. M. “Thermal Analysis - Theory and Applications in Metalcasting”. In: *International Journal of Metalcasting* 9.1 (2015), pp. 7–22. ISSN: 1939-5981 (cit. on p. 14).

[34] D’Avignon, K. and Kummert, M. “Assessment of T-History Method Variants to Obtain Enthalpy-Temperature Curves for PCMs With Significant Subcooling”. In: *Journal of Thermal Science and Engineering Applications* (2015). ISSN: 1948-5085. DOI: 10.1115/1.4031220 (cit. on p. 14).

[35] Cabeza, L. F. et al. “Key performance indicators in thermal energy storage: Survey and assessment”. In: *Renewable Energy* 83 (2015), pp. 820–827. ISSN: 09601481. DOI: 10.1016/j.renene.2015.05.019 (cit. on p. 14).

[36] Gschwander, S. et al. “Standardization of PCM Characterization via DSC”. In: *Greenstock 2015*. 2015 (cit. on p. 14).

[37] Zhang, Y. et al. “A simple method, the T-history method, of determining the heat of fusion, specific heat and thermal conductivity of phase-change materials”. In: *Measurement Science and Technology* 10.3 (1999), p. 201. ISSN: 0957-0233 (cit. on p. 15).

[38] Solé, A. et al. “Review of the T-history method to determine thermophysical properties of phase change materials (PCM)”. In: *Renewable and Sustainable Energy Reviews* 26 (2013), pp. 425–436. ISSN: 13640321. DOI: 10.1016/j.rser.2013.05.066 (cit. on p. 15).

[39] Rathgeber, C. et al. “Enthalpy-temperature plots to compare calorimetric measurements of phase change materials at different sample scales”. In: *Journal of Energy Storage* 15 (2018), pp. 32–38. ISSN: 2352152X. DOI: 10.1016/j.est.2017.11.002 (cit. on p. 15).

[40] Hiebler, S. “Kalorimetrische Methoden zur Bestimmung der Enthalpie von Latentwärmespeichermaterialien während des Phasenübergangs: (in German)”. PhD thesis. TUM, 2007 (cit. on pp. 15–17).

[41] Badenhorst, H. and Cabeza, L. F. “Critical analysis of the T-history method: A fundamental approach”. In: *Thermochimica Acta* (2017). ISSN: 0040-6031. DOI: 10.1016/j.tca.2017.02.005 (cit. on p. 17).

[42] Lázaro, A. et al. “Verification of a T-history installation to measure enthalpy versus temperature curves of phase change materials”. In: *Measurement Science and Technology* 17.8 (2006), pp. 2168–2174. ISSN: 0957-0233. DOI: 10.1088/0957-0233/17/8/016 (cit. on p. 17).

[43] Eilers, P. H. C. “A Perfect Smoother”. In: *Analytical Chemistry* 75.14 (2003), pp. 3631–3636. ISSN: 0003-2700. DOI: 10.1021/ac034173t (cit. on p. 22).

[44] Stickel, J. J. "Data smoothing and numerical differentiation by a regularization method". In: *Computers & Chemical Engineering* 34.4 (2010), pp. 467–475. ISSN: 00981354. DOI: 10.1016/j.compchemeng.2009.10.007 (cit. on p. 22).

[45] Joint Committee for Guides in Metrology. *Evaluation of measurement data - Supplement 1 to the "Guide to the expression of uncertainty in measurement": Propagation of distributions using a Monte Carlo method: JCGM 101:2008*. 2008 (cit. on p. 23).

[46] Voller, V. R. and Swaminathan, C. R. "General Source-Based Method for Solidification Phase Change". In: *Numerical Heat Transfer, Part B: Fundamentals* 19.2 (1991), pp. 175–189. ISSN: 1040-7790. DOI: 10.1080/10407799108944962 (cit. on pp. 25, 27, 31–33).

[47] Pointner, H. et al. "Computational efficiency in numerical modeling of high temperature latent heat storage: Comparison of selected software tools based on experimental data". In: *Applied Energy* 161 (2016), pp. 337–348. ISSN: 03062619. DOI: 10.1016/j.apenergy.2015.10.020 (cit. on p. 27).

[48] Andersson, B. et al. *Computational fluid dynamics for engineers*. Cambridge and New York: Cambridge University Press, 2011. ISBN: 1139093592 (cit. on pp. 28–31, 34).

[49] Patankar, S. V. *Numerical heat transfer and fluid flow*. Series in computational and physical processes in mechanics and thermal sciences. Great Britain: Taylor & Francis, 1980. ISBN: 0891165223 (cit. on pp. 29, 31).

[50] *VDI Heat Atlas: with 539 tables*. 2. ed. Springer reference. Heidelberg: Springer, 2010. ISBN: 9783540778769 (cit. on pp. 31, 35, 50).

[51] Glicksman, M. E. *Principles of solidification: An introduction to modern casting and crystal growth concepts*. New York: Springer, 2011. ISBN: 1441973443 (cit. on p. 41).

[52] Stefanescu, D. M. *Science and Engineering of Casting Solidification*. 3rd ed. 2015. SpringerLink : Bücher. Cham: Springer, 2015. ISBN: 3319156934 (cit. on p. 41).

[53] Verma, P. et al. "Review of mathematical modeling on latent heat thermal energy storage systems using phase-change material". In: *Renewable and Sustainable Energy Reviews* 12.4 (2008), pp. 999–1031. ISSN: 13640321. DOI: 10.1016/j.rser.2006.11.002 (cit. on p. 41).

[54] Uzan, A. Y. et al. "A novel multi-dimensional model for solidification process with supercooling". In: *International Journal of Heat and Mass Transfer* 106 (2017), pp. 91–102. ISSN: 0017-9310. DOI: 10.1016/j.ijheatmasstransfer.2016.10.046 (cit. on p. 41).

[55] Bajura, R. A. and Jones, E. H. "Flow Distribution Manifolds". In: *Journal of Fluids Engineering* 98.4 (1976), p. 654. ISSN: 00982202. DOI: 10.1115/1.3448441 (cit. on p. 41).

[56] Lacroix, M. "Numerical simulation of a shell-and-tube latent heat thermal energy storage unit". In: *Solar Energy* 50.4 (1993), pp. 357–367. ISSN: 0038092X. DOI: 10.1016/0038-092X(93)90029-N (cit. on pp. 34, 35).

[57] Tan, P. et al. "Correction of the enthalpy–temperature curve of phase change materials obtained from the T-History method based on a transient heat conduction model". In: *International Journal of Heat and Mass Transfer* 105 (2017), pp. 573–588. ISSN: 0017-9310. DOI: 10.1016/j.ijheatmasstransfer.2016.10.001 (cit. on pp. 35, 50).

[58] Li, P. et al. "Similarity and generalized analysis of efficiencies of thermal energy storage systems". In: *Renewable Energy* 39.1 (2012), pp. 388–402. ISSN: 09601481. DOI: 10.1016/j.renene.2011.08.032 (cit. on pp. 45, 47).

[59] Amin, N. et al. "Optimising PCM thermal storage systems for maximum energy storage effectiveness". In: *Solar Energy* 86.9 (2012), pp. 2263–2272. ISSN: 0038092X. DOI: 10.1016/j.solener.2012.04.020 (cit. on pp. 45, 47).

[60] Tay, N. et al. "Designing a PCM storage system using the effectiveness-number of transfer units method in low energy cooling of buildings". In: *Energy and Buildings* 50 (2012), pp. 234–242. ISSN: 03787788. DOI: 10.1016/j.enbuild.2012.03.041 (cit. on p. 47).

[61] Tay, N. et al. "An effectiveness-NTU technique for characterising tube-in-tank phase change thermal energy storage systems". In: *Applied Energy* 91.1 (2012), pp. 309–319. ISSN: 03062619. DOI: 10.1016/j.apenergy.2011.09.039 (cit. on p. 47).

[62] Belusko, M. et al. "Characterising PCM thermal storage systems using the effectiveness-NTU approach". In: *International Journal of Heat and Mass Transfer* 55.13-14 (2012), pp. 3359–3365. ISSN: 0017-9310. DOI: 10.1016/j.ijheatmasstransfer.2012.03.018 (cit. on p. 55).

[63] Rubitherm GmbH. *RT10HC Data Sheet*. 2016. URL: https://www.rubitherm.eu/media/products/datasheets/Techdata_-RT10HC_EN_31052016.PDF (cit. on p. 58).